Violating the Weak Cosmic Censorship Conjecture in Asymptotically Anti-de Sitter Space-Times

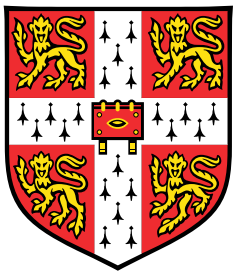

Toby Crisford

Department of Applied Mathematics and Theoretical Physics
University of Cambridge

This dissertation is submitted for the degree of
Doctor of Philosophy

King's College

August 2019

This thesis is dedicated to my grandfather,
John Thorn (1923 - 2017)

Declaration

This dissertation is the result of my own work and includes nothing which is the outcome of work done in collaboration except as declared in the Preface and specified in the text. It is not substantially the same as any that I have submitted, or, is being concurrently submitted for a degree or diploma or other qualification at the University of Cambridge or any other University or similar institution except as declared in the Preface and specified in the text. I further state that no substantial part of my dissertation has already been submitted, or, is being concurrently submitted for any such degree, diploma or other qualification at the University of Cambridge or any other University or similar institution except as declared in the Preface and specified in the text.

Toby Crisford
August 2019

Acknowledgements

First and foremost, I thank my supervisor Jorge Santos, who has been a constant source of advice and support. His encouragement and enthusiasm have made completing this PhD a real pleasure. I also thank Gary Horowitz for his valuable guidance and input. It has been a privilege to work with him.

Thank you to all of the PhD students of Pavilion B whose company and bizarre lunchtime discussions helped to make my time there so enjoyable, and from whom I learnt so much. I especially thank my officemates, Charles and Roxana. Together we invented and participated in the fun office games of "Highest Number" and "Chair Wars" which often provided a welcome break from physics.

Throughout my time as a PhD student, I have been lucky to share a home with my good friends Atticus, Fingal, Huw, Jas, Jo, and Rafi. I owe a special thanks to them for helping to make this time a true treasure trove of happy memories.

I would also like to thank my family, and especially my parents. I would not have reached this point without their love and generosity. Finally, I thank my brother Ben for his wisdom.

Abstract

We numerically construct solutions to four dimensional General Relativity with negative cosmological constant, both with and without an electromagnetic field. Our results suggest that in both cases the space-time curvature can be made to grow without bound in a region visible to distant observers by imposing sufficiently violent boundary conditions on the metric or gauge field. In the electromagnetic case, this only happens at zero temperature, and we present a new numerical scheme capable of performing time evolution in this context. We argue that our results, at least in the electromagnetic case, violate the spirit of the Weak Cosmic Censorship Conjecture, so that this conjecture fails in $3+1$ dimensional asymptotically Anti de-Sitter spaces. We then argue that if charged fields are included with a sufficiently large charge relative to their mass, cosmic censorship appears to be restored. The minimal charge agrees precisely with the bound given by the Weak Gravity Conjecture, suggesting an intriguing connection between this conjecture and cosmic censorship. More generally, we propose that "large" naked singularities, where the curvature becomes large over a large region of space, will be forbidden in any theory which can be completed into quantum gravity in the UV.

Table of contents

Chapter 1

Introduction

Over one hundred years since its inception, General Relativity (GR) remains the best description of gravity that we have. In GR, the gravitational field is described by a set of non-linear partial differential equations, collectively referred to as Einstein's equation. Constructing solutions to these non-linear equations is a challenging problem, and up until the 1980s, the known solutions typically contained a large amount of symmetry. However, over the last few decades the situation has been transformed by dramatic improvements in the power of computers. It is now possible to use numerical analysis techniques to construct interesting solutions to Einstein's equation with few simplifying assumptions. In this thesis, we present two new classes of solution that have been obtained in this way. Both are $3+1$ dimensional and asymptotically Anti-de Sitter. The first is in vacuum, and the second contains an electromagnetic field. These solutions are significant because, in each case, we find evidence that the space-time curvature can be made to grow without bound in a region visible to distant observers.

One of the most important open problems in GR is to prove, or disprove, the Weak Cosmic Censorship Conjecture. This conjecture claims that, under a modest set of conditions, the formation of *naked singularities* is impossible in GR [49]. We review the conjecture in detail in Chapter 2, but roughly, naked singularities can be thought of as places with infinite curvature that are visible to distant observers. Our solutions do not contain naked singularities in this sense, since the curvature does not become infinite in finite time. However, the curvature does become arbitrarily large, and we will argue that our electromagnetic solutions at least do violate the Weak Cosmic Censorship Conjecture in spirit. The evidence in the vacuum case is weaker. We claim that the Weak Cosmic Censorship Conjecture therefore does not hold in $3+1$ dimensional asymptotically Anti-de Sitter spaces.

Interestingly, we find that in order for our electromagnetic solutions to violate cosmic censorship, it is essential that any charged fields have small charge relative to their mass. If

the charge is large, then large naked curvatures are avoided. What's more, the minimal charge necessary to protect cosmic censorship appears to agree precisely with the minimal charge stipulated by the Weak Gravity Conjecture, one of the so called Swampland conjectures of String Theory. The Weak Gravity Conjecture asserts that any low energy effective theory can only have a UV completion into quantum gravity if it contains a charged particle of sufficiently large charge relative to its mass [1]. This potential connection [55] between the two conjectures is intriguing, and it is tempting to suggest that generically the Weak Cosmic Censorship Conjecture will hold in any theory which *can* be completed into quantum gravity in the UV.

There are other proposed violations of cosmic censorship which seem to contradict this suggestion. The Weak Cosmic Censorship Conjecture fails in higher dimensions through the Gregory-Laflamme instability [27], and superradiance might provide an alternative mechanism that causes it to fail in $3+1$ dimensional asymptotically Anti de-Sitter space in vacuum [46, 7], yet a consistent quantum gravity completion can likely be found in both cases. However, the naked singularities arising in these examples are "small". The curvature becomes arbitrarily large in an arbitrarily small region of the space time. Our examples are more violent, with the curvature becoming large over a large region of the space time. Having strengthened the Weak Cosmic Censorship Conjecture by extending it to cover large finite curvatures, we will now suggest weakening it. While "small" naked singularities might sometimes be allowed, perhaps "large" naked singularities will always be forbidden in theories which are the low energy effective description of a consistent quantum gravity theory in the UV.

The rest of this thesis is organised as follows. In Chapter 2 we review the Weak Cosmic Censorship Conjecture, and explain how it can be applied in asymptotically Anti-de Sitter spaces. In Chapter 3 we review a numerical method [3] which can be applied to solve time dependent problems in asymptotically Anti-de Sitter spaces at finite temperature. In Chapter 4 we present original work showing how this method can be adapted to cope with a broader class of problems, including those at zero temperature. Chapter 5 contains the vacuum solutions and is based on the publication [14]. This work was carried out in collaboration with Jorge E. Santos (JES) and Gary T. Horowitz (GTH). Chapter 6 contains the electromagnetic solutions, and is based on the publication [15], a collaboration with JES. Finally, in Chapter 7 we give evidence for a connection between the Weak Gravity Conjecture and Weak Cosmic Censorship. This Chapter is based on the publication [13] and contains work carried out in collaboration with JES and GTH. Where numerical results are presented, time dependent solutions were produced by the author, and stationary solutions by JES, unless otherwise stated.

Chapter 2

The Weak Cosmic Censorship Conjecture

The Weak Cosmic Censorship Conjecture (WCCC) roughly says that whenever a singularity forms, it should be contained inside a black hole [59]. Before discussing the motivation for and significance of the WCCC, we begin by briefly reviewing the definition of a singularity and the definition of a black hole.

A singularity can be heuristically understood as a "hole" in the space-time [58]. Converting this intuition into a precise mathematical definition is notoriously difficult, but the standard approach is to say that a space-time is singular if there are geodesics which terminate in finite affine length. If this was true of a time-like geodesic, then a freely falling observer could encounter the edge of the space-time in finite proper time. This is a puzzling prediction for a theory to make. However, the examples we consider will typically be *curvature* singularities. A curvature invariant blows up as the singularity is approached. This helps us make sense of how these singularities should be interpreted: in the high curvature regime tidal forces become very large and new unknown physics becomes important. It should not be surprising that GR predicts such singularities, since it is a classical theory and we expect it to be only an effective description of nature at large scales. The equations of fluid dynamics also predict their own downfall in a similar way.

A more unfamiliar prediction of GR is that of a black hole. In asymptotically flat space, a black hole is a region which does not lie in the causal past of future null infinity, $\mathscr{I}^+$. The boundary of this region is known as the black hole horizon. It is therefore not possible for any observer outside of the black hole horizon to receive information from an event inside the black hole. In particular, if a singularity is contained inside a black hole then it will not be visible to observers outside.

Both singularities and black holes have been important objects of study in GR ever since the first non-trivial solution to Einstein's equation was written down by Schwarzschild [51]. The Schwarzschild solution is the spherically symmetric stationary vacuum solution to Einstein's equation, and contains both a curvature singularity and a black hole region. Importantly, the singularity *is* contained inside the black hole. The same is true of the Kerr solution [41] (which is stationary but not spherically symmetric). For a long time it was not clear which features of these solutions might have astrophysical relevance, and which were merely unphysical consequences of the simplifying assumptions. The celebrated singularity theorem of Penrose [48] ultimately proved that singularities would generically be produced in sufficiently violent gravitational collapse, even if perturbations break the spherical symmetry[1]. This left open the question: would these singularities generically be hidden inside black holes, as in Schwarzschild and Kerr, or might they be "naked"? Penrose proposed that singularities would never be naked [49]. A "Cosmic Censor" would always hide them inside a black hole. This proposal led to what we now call the Weak Cosmic Censorship Conjecture (WCCC), the precise statement of which shall be reviewed shortly.

The WCCC, if true, could be viewed as both a blessing and a curse. On the one hand it means that we do not have to worry about the unknown physics of the singularity in order to make predictions in astrophysics. Whatever goes on at the singularity, the WCCC means that it can have no observable consequences for anyone outside the black hole. If, for example, we want to model the collision of two black holes, then all we need is the classical vacuum Einstein equation. Numerical simulations have been able to predict the gravitational wave signals which have now been observed by LIGO. On the other hand, this same feature could be viewed as a curse. If we want to learn about the new physics which takes over when the curvature becomes large, presumably a quantum theory of gravity, then a black hole singularity would be an ideal place to look. However, the WCCC tells us that we cannot extract any information about what goes on there unless we jump into a black hole. It is as if nature is conspiring to hide the effects of quantum gravity from us. If this really is the case, it could be hinting at something deep about the nature of quantum gravity.

In this chapter we first review the WCCC in asymptotically flat space and present some evidence that has been put forward to support it. We then review asymptotically Anti-de Sitter space and explain how the WCCC can be adapted to cover these spaces as well.

[1] However, these theorems do not guarantee that the singularity will be a *curvature* singularity.

2.1 Precise formulation of the WCCC

The statement that *it is impossible to form a naked singularity* can be formulated more precisely as follows

Conjecture 2.1.1. *The maximal Cauchy evolution of asymptotically flat initial data is asymptotically flat and strongly asymptotically predictable [22].*

This captures the intuition that if we want to predict everything that happens outside of the black hole region, then Einstein's equation (along with the relevant matter equations of motion) are all we need in order to do this. Strong asymptotic predictability means that there exists an open set in the conformal compactification of the space-time which contains the exterior of all black hole regions as well as all black hole horizons, such that this set is globally hyperbolic. In other words, we can predict everything on and outside of the black hole horizons. A naked singularity cannot form if this conjecture is true, because if a null geodesic connected an event outside of the black holes to a singularity, then this geodesic would not intersect the initial data, and a globally hyperbolic open set of the form required by strong asymptotic predictability would not exist.

The problem with the conjecture as stated is that it can be shown to be false. In order for the WCCC to have a chance of being true, we must add a number of conditions in order to rule out classes of non-physical counter-examples. We now discuss each of these conditions in turn.

- *The initial data must be geodesically complete.* This requirement is easy to understand. There do exist solutions to Einstein's equation containing naked singularities. One example is the unphysical negative mass Schwarzschild solution. Other examples include the cosmological solutions which have been put forward to describe our universe, since the initial Big Bang singularity is visible to all observers. The WCCC can therefore only be true if it asserts that it is impossible to *form* a naked singularity if you do not begin with any singularity initially. We must require that there are no singularities already contained in our initial data.

- *Non-generic counter-examples are allowed.* If you are allowed to fine tune the initial data, then it is possible to form naked singularities. The standard example of this is critical gravitational collapse. The gravitational collapse of a massless scalar field in spherical symmetry was studied analytically by Christodoulou [10], and numerically by Choptuik [8]. If the initial amplitude of the scalar field profile (described by a parameter p) is small, then the scalar field eventually disperses. If p is large, then a black hole is formed. There is a critical value, p^*, which separates these two regimes.

When $p = p^*$ precisely, a naked singularity forms. This appears to contradict the WCCC, but if such a critical solution is perturbed slightly, then either the singularity will disappear, or a black hole will form to hide it. We therefore do not expect this counter-example to be physically relevant, and we should refine the conjecture to allow for such non-generic exceptions. To violate the refined version of the conjecture, it is not enough to find a single solution which produces a naked singularity, as in critical collapse. We must find an open set of such solutions. For the collapse of a massless scalar field in spherical symmetry Christoudoulou has rigorously proven that the generic version of the WCCC does in fact hold [11].

- *The matter fields must be suitably well behaved.* Since the WCCC remains unproven even in vacuum, it is unclear precisely what minimal conditions the matter fields will need to satisfy in order for the WCCC to hold. But for the WCCC to be physically interesting, they should not be too restrictive. One condition that certainly is required is that the matter equations of motion have a well posed initial value formulation. Another is that the stress tensor obeys the dominant energy condition: $-T^a{}_b V^b$ is a future directed causal vector for all future directed timelike V^a. A consequence of the dominant energy condition is that the energy density of matter is always nonnegative. It makes sense that we need to impose this, since otherwise we might be able to use the matter to form a negative mass Schwarzschild black hole, which would contain a naked singularity. Physically reasonable matter is expected to obey the dominant energy condition.

  These conditions alone do not appear to be sufficient however. Christoudoulou has shown that generic (at least within spherical symmetry) counter-examples to the WCCC exist for "dust" matter [9], which has a pressureless stress tensor. Such an equation of state is not thought to be physically realistic, and it could lead to singularity formation even if evolved in a flat background uncoupled from gravity [59]. This suggests that we should impose a further condition: the matter fields should not produce singularities if evolved in a fixed globally hyperbolic background space-time from regular initial data [59]. This condition rules out some physically relevant matter, such as fluids, but it guarantees that any naked singularities which form are gravitational in origin. The fact that fluid singularities can be visible should be no surprise and should have nothing to do with the validity of the WCCC.

- *The number of space-time dimensions must be 3+1.* This is clearly not an unreasonable condition from a physical point of view, but it is interesting that it appears to be necessary. As soon as you go to $4+1$ dimensions or above, there exist asymptotically

flat black hole solutions with non-spherical topology. In particular, in $4+1$ dimensions there exist so called "black ring" ($S^1 \times S^2$) [17] solutions. Unlike their $3+1$ dimensional counterparts, these black holes are unstable to the Gregory-Laflamme instability [27]. Numerical studies have confirmed that the apparent horizon of a black ring will pinch off in finite time [42, 20], appearing to result in a naked singularity. One limitation of these numerical studies is that it is only possible to track the apparent horizon, not the true event horizon. Another limitation is that you must begin with an unstable black hole solution, and it is not clear that such a black hole could ever be formed in the first place. Nevertheless, it seems very likely that the WCCC fails to hold in higher dimensions.

2.2 Evidence in favour of the WCCC

Although the WCCC has still not been proven, there is now convincing evidence that it is true in asymptotically flat $3+1$ dimensional space-times. This evidence comes from investigating the many cases where the WCCC might have been violated, and consistently finding that it instead holds firm:

- For the special case of a massless scalar field with spherical symmetry, Christoudoulou has proven that the WCCC is true [11].

- The study of linear perturbations to the Schwarzschild [56] and Kerr [60] black hole solutions has established their *mode stability*, meaning that fixed mode perturbations always decay. More recently, it has been proven that the Schwarzschild solution is stable for arbitrary linear perturbations [16]. This makes these solutions good candidates for the endpoint of gravitational collapse, with their singularities safely hidden behind a horizon. If they had been found to have unstable modes, or to be otherwise linearly unstable, then this would have indicated that naked singularities almost certainly can form, as is thought to be the case for black rings.

- The WCCC can be used to derive a constraint on initial data known as the Penrose inequality, assuming that the evolution eventually settles down to a Kerr black hole. The WCCC implies that an apparent horizon must be contained inside an event horizon in order that the resulting singularity is not naked, the total event horizon area must increase in time by Hawking's area theorem, the area of the final stationary black hole is bounded above by the final mass, and the mass must be less than the initial energy of the system (some energy can be radiated to infinity). Putting all this together gives the Penrose inequality, a bound on the initial apparent horizon area by the initial energy.

Despite many attempts, no initial data has been found which violates this inequality. In the case of null dust, it has actually been proven that the inequality will hold for all initial data [24].

- By now, there are many numerical studies of the full non-linear Einstein equation in regimes far from any known analytical solution. For example, black hole collisions can now be studied numerically [45]. In all cases looked at so far, no violation of the WCCC has ever been observed. Singularities have always been hidden inside black holes.

- Finally, evidence in favour of the WCCC comes from the failure of attempts to overspin or overcharge a black hole. Both the Kerr solution, and the Reissner-Nordstrom solution (a black hole with electric charge), develop a naked singularity when the spin, or the charge, is increased beyond the extremal value. This suggests a possible way to violate the WCCC [57, 52]: we try to throw a particle with spin, or charge, into a black hole such that if it is captured, it will push the spin, or charge, of the black hole beyond its extremal limit. However, attempts to do this run into the problem that as the black hole approaches the extremal limit, it tends to repel particles with the same spin or charge more and more strongly. Overspinning or overcharging a black hole appears to be impossible.

2.3 The WCCC in Asymptotically Anti-de Sitter Space

There is now compelling evidence from a variety of different lines of research that the WCCC is true in asymptotically flat space, but the subject of this thesis is the status of the WCCC in asymptotically Anti-de Sitter (AdS) space. We will need to generalize the statement of the WCCC so that it can be applied in AdS, and the obvious question is: why bother? Our universe does not appear to be asymptotically AdS[2], and we have already seen that a number of conditions are required in the statement of the WCCC to rule out non-physical counter-examples. If we find that our generalized form of the WCCC is violated in AdS, it seems that all that means is that we will just have to add one more condition to this long list. Why is that worth doing?

There are a number of answers that can be given to this question. First, the WCCC remains unproven, and is an active field of research. Exploring the necessary conditions

[2]Our universe is not asymptotically flat either, but asymptotically flat space-times are thought to be good models for isolated gravitational systems, so that a counter-example to the WCCC in asymptotically flat space would have astrophysical significance.

that are required for it to hold will help to improve our overall understanding of cosmic censorship, which is important. For example, one could imagine a counter-example to the WCCC in AdS motivating the construction of a counter-example in flat space, or inspiring a new argument for why it should hold (although this is not something that we have been able to do in this thesis).

Second, if there really is a deep reason for *why* the WCCC is true[3], coming from as yet unknown physics, then non-physical counter-examples to the WCCC would take on a new fascinating significance. For example, if we understood why the precise statement of the WCCC given previously must be true, then knowing that it is false in 5 dimensions or more means that we would have also understood why the universe we live in has fewer than 5 dimensions. Similarly, finding a counter-example in AdS would mean that a deeper understanding of cosmic censorship might explain why the universe we live in is not AdS. These would be extremely important results, and such scenarios are probably unrealistic. There is unlikely to be a deep quantum gravity reason for why the precise statement of the WCCC is true (if it is indeed true) since it seems to be possible to construct consistent quantum gravity theories in 10 dimensions (described by string theory) where the WCCC does not hold. However, we will argue later that such naked singularities are "mild", and a weaker version of the WCCC ruling out only "large" naked singularities might indeed be a deep principle with its origins in quantum gravity. This weaker version might hold not only in higher dimensions, but also in AdS. The AdS counter-examples we find would then need to be non-physical for some reason (other than their AdS asymptotics), and this will lead to the fascinating possibility of connecting cosmic censorship with the Weak Gravity Conjecture (WGC), one of the so-called "swampland" conjectures of string theory. If this story is correct, then a deep understanding of cosmic censorship might not tell us why we live in $3+1$ dimensions, or why we do not live in AdS, but it would help to improve our understanding of why the WGC is true. Conversely, a better understanding of the swampland conjectures might improve our understanding of cosmic censorship.

Finally, asymptotically AdS space-times have a special significance because of the AdS/CFT correspondence. This correspondence is one of the most important developments in fundamental physics in the last few decades. It says that a non-gravitational gauge theory in d space-time dimensions can be dual to a gravitational theory (in particular a string theory) in $d+1$ dimensional asymptotically AdS space [44]. What's more, a strong coupling large N regime in the gauge theory corresponds to a tractable weakly coupled gravitational theory which can be described with classical equations of motion. Conversely, when the string

[3]Here we have in mind not a formal mathematical proof within the framework of GR, but a physical reason coming from a higher energy theory.

coupling and string length are large, the gauge theory is weakly coupled and tractable, giving a way of doing quantum gravity outside of the perturbative regime. It has therefore become more important to understand the behaviour of gravity in asymptotically AdS space-times, and understanding the status of the WCCC should be a part of that. For example, if we were able to form a naked singularity in AdS, then we would want to ask what this looked like in the boundary theory, and whether we could learn anything about how the singularity is resolved within quantum gravity. Unfortunately, though we will find counter-examples to the WCCC in AdS, the "large" ones only appear to be present when no consistent quantum description exists at high energies, ruling out an investigation of these naked singularities using the AdS/CFT correspondence.

2.3.1 A Brief Review of AdS Space

AdS space is the maximally symmetric vacuum solution to Einstein's equation with a negative cosmological constant. The metric for $d+1$ dimensional AdS space can be written in the following form

$$ds^2 = -\left(1+\frac{r^2}{L^2}\right)dt^2 + \left(1+\frac{r^2}{L^2}\right)^{-1} dr^2 + r^2 d\Omega_{d-1}^2 \tag{2.1}$$

which makes the $SO(d)$ symmetry of the space-time (a subgroup of the full isometry group) manifest. L, a characteristic length scale associated with the curvature, is related to the cosmological constant by

$$\Lambda = -\frac{d(d-1)}{2L^2}. \tag{2.2}$$

Conformal compactification can be applied to the r coordinate to give a Penrose diagram for the space-time, which turns out to be a cylinder, shown in Figure 2.1.

One important feature which distinguishes AdS from flat space, is that the boundary at $r=\infty$ is timelike. This means that there is no Cauchy surface. If we wish to perform dynamical evolution in an asymptotically AdS space-time, there will always be points whose past light cone intersects the boundary before it intersects the initial data. Therefore, as well as providing initial conditions, to solve Einstein's equation in asymptotically AdS space-times we must also provide boundary conditions for each of our fields at $r=\infty$. Typically, the boundary conditions we impose will cause waves that reach the boundary to be reflected back into the bulk. For this reason, AdS space is sometimes referred to as a "covariant box". It gives us a way of putting "walls" around a gravitational system without breaking local Lorentz invariance anywhere. These reflecting walls give rise to new kinds of gravitational physics, and this will play a crucial role in our proposed violations of the WCCC.

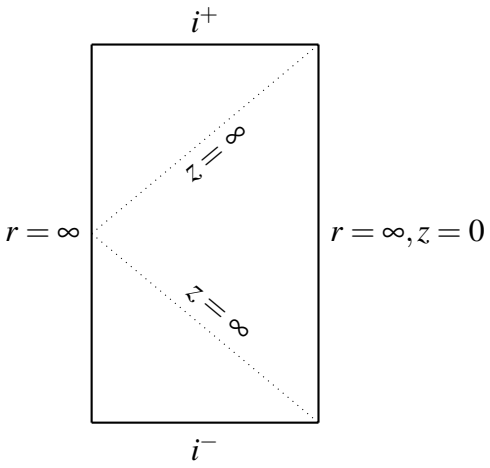

Fig. 2.1 The Penrose diagram for AdS. The triangular region bounded by the dotted lines is the Poincaré patch.

It is common to work in a smaller patch of the full AdS space-time, marked by the dotted lines in Figure 2.1. This is known as the Poincaré patch, while the full AdS space-time is often referred to as *global* AdS. We can choose coordinates covering this patch so that the metric is placed in the following simple form

$$ds^2 = \frac{L^2}{z^2}\left(dz^2 + \eta_{\mu\nu}dx^\mu dx^\nu\right). \tag{2.3}$$

The advantage we get by thinking in terms of these coordinates is that any constant z surface is flat. The metric restricted to a constant z surface is just $\eta_{\mu\nu}$, the Minkowski metric, scaled by an overall factor. The coordinate z, referred to as the bulk radial coordinate, tells us how deep we are in the bulk. The AdS boundary lies at $z = 0$, and the dotted lines in Figure 2.1 lie at $z = \infty$, a surface referred to as the Poincaré horizon. The word "horizon" is appropriate here because this surface separates points which are in causal contact with the boundary of the Poincaré patch from those which are not.

So far we have discussed AdS space as the maximally symmetric solution to Einstein's equation with negative cosmological constant, but we are really interested in the behaviour of solutions which are only *asymptotically* AdS, which means that they approach AdS near their timelike boundary[4]. We will eventually construct such solutions numerically, but there are some important asymptotically AdS solutions which are known analytically. These are the analogues of the Schwarzschild, Reissner-Nordstrom, and Kerr black holes from asymptotically flat space.

[4]We will even consider still more general solutions, where the boundary metric can also be deformed, giving rise to solutions described as *asymptotically locally AdS*.

Unlike in asymptotically flat space, where it has been proven that all black holes in $3+1$ dimensions have spherical topology, black holes in asymptotically AdS space can have both spherical and planar topology. The metrics for spherical and planar AdS-Schwarzschild black holes are given below[5]

$$ds^2 = -\left(1 - \frac{2M}{r^{d-2}} + \frac{r^2}{L^2}\right) dt^2 + \left(1 - \frac{2M}{r^{d-2}} + \frac{r^2}{L^2}\right)^{-1} dr^2 + r^2 d\Omega_{d-1}^2 \tag{2.4}$$

$$ds^2 = \frac{L^2}{z^2}\left[-\left(1 - L^{-2d+2} M z^d\right) dt^2 + \left(1 - L^{-2d+2} M z^d\right)^{-1} dz^2 + \delta_{ij} dx^i dx^j\right]. \tag{2.5}$$

Note that if we set $M = 0$, the spherical black hole metric reduces to the AdS metric given in Equation 2.1. We can think of the size of the spherical black hole shrinking to zero as $M \to 0$. On the other hand, the planar black hole metric reduces to the metric for the Poincaré patch given in Equation 2.3. We can think of the Poincaré patch as the zero temperature limit of the exterior of a planar AdS-Schwarzschild black hole, with the Poincaré horizon a zero temperature black hole horizon. It is important to stress that while the metrics 2.1 and 2.3 describe the same space-time (the second describes a subset of the first), the same is not true of the spherical and planar black hole metrics given above. This tells us that if we deform the Poincaré patch metric given in 2.3, we can end up with an asymptotically AdS solution that cannot be interpreted in terms of the global AdS picture.

We conclude this section by considering one particular example of a phenomenon that is dramatically altered by the presence of a timelike boundary: superradiance. Before discussing superradiance, recall the Penrose process for particles [50]. Rotating black holes contain an ergoregion outside of their event horizon where the Killing field generating asymptotic time translations becomes space-like. It is therefore possible for a time-like geodesic in this region to have negative energy. In particular, a particle can fall into this region with positive energy and split in two, producing one particle with negative energy and one with a larger positive energy than was present initially. The negative energy particle must be captured by the black hole, but the positive energy particle can escape. When backreaction is taken into account, the mass of the black hole must be reduced, and we have in effect extracted energy from the black hole through what is known as the Penrose process.

The same procedure can occur with solutions to the wave equation on a rotating black hole background, where it is known as superradiance [64, 53]. Through superradiance, it is possible for a wave to extract energy from a black hole. In asymptotically flat space, if we send a massless wave towards a black hole then it will return with more energy before escaping to infinity. But in an asymptotically AdS space-time, there is nowhere for it to

[5] A third possibility, with a hyperbolic horizon, is omitted.

escape to. When it hits the time-like boundary it will be reflected back towards the black hole. This is the origin of the runaway process known as the superradiant instability. Rotating black holes in asymptotically AdS space can therefore be unstable [32, 6] (though not all are), unlike their counterparts in asymptotically flat space.

The stability of black holes was one of the key pieces of evidence in favour of the WCCC in asymptotically flat space-times. The fact that it fails to hold in AdS should already cause us to doubt the validity of the WCCC in that regime. Indeed, it has been proposed that the endpoint of the superradiant instability for AdS-Kerr black holes will lead to naked singularity formation and the violation of the WCCC [46], though these are not the counter-examples we will consider in this thesis. If naked singularities form during superradiance, they are likely to be mild, in the same family as those arising from the Gregory-Laflamme instability. The naked singularities we present are "large" (the curvature grows over a large region of the space-time).

2.3.2 A Brief Review of AdS/CFT

Much of the current interest in asymptotically AdS space-times comes from the AdS/CFT correspondence. In its original form, the AdS/CFT correspondence is a conjectured duality between Type IIB Superstring theory in an $AdS_5 \times S^5$ background (the bulk) and $\mathcal{N} = 4$ Super Yang-Mills theory with gauge group $SU(N)$ living on its $3+1$ dimensional boundary [44, 62, 29]. The large N, strong coupling limit of the gauge theory corresponds to the classical, weak coupling limit of the string theory, where a classical supergravity description is appropriate. The AdS/CFT correspondence is often referred to as "holography" because of the different number of space-time dimensions in the two theories. The original conjecture has been generalized to cover different theories with different numbers of space-time dimensions, but the idea is always that a string theory in $AdS_{d+1} \times$ "some compactification" is dual to a conformal gauge theory living on its d dimensional boundary[6] [43]. One check on the validity of the conjecture is that the symmetries of each theory match. The full isometry group of AdS_{d+1} is $SO(2,d)$, and this is also the group of conformal transformations in d dimensions. Thinking of the d dimensional space-time as the boundary of AdS makes this equivalence manifest: an isometry of AdS acts on the AdS boundary as a conformal transformation.

The statement that two theories are *dual* is, in this context, the assertion that they really describe the same underlying physics. There should be a dictionary which tells you how to write states of one theory as states of the other, and this dictionary should have the property

[6] This is the picture at least up to $d = 6$. Beyond this point no interacting superconformal field theories exist.

that it commutes with the dynamics. For example, suppose theory 1 begins in state A, and the dictionary tells you that this is equivalent to state $D(A)$ in theory 2. If at a later time theory 1 is in state A', then theory 2 should be in state $D(A')$.

The AdS/CFT correspondence remains a conjecture, and a complete understanding of the dictionary is lacking. Part of the problem is that string theory is not well understood outside of the perturbative regime. Nevertheless, some aspects of the dictionary have been made precise. First, we know that we have to provide boundary conditions for each of the fields in the bulk in the classical limit, and so we can ask what the interpretation of this will be on the boundary. A natural assumption is that the boundary conditions for fields in the classical gravity theory become sources for operators in the boundary theory [62, 29], since boundary conditions and sources play a similar role: they can be freely specified and that then determines the dynamics. Applying this idea to a bulk scalar field ϕ, and equating the partition functions of the two theories (if they contain the same states obeying the same dynamics then their partition functions should be equal) we get a part of the holographic dictionary

$$\left\langle \exp \int \phi_0 \mathscr{O} \right\rangle_{\text{CFT}} = Z_S(\phi_0). \tag{2.6}$$

The left-hand side is the partition function of the CFT with a source ϕ_0 included for some local operator $\mathscr{O}$, and the right-hand side is the bulk partition function with boundary condition ϕ_0 applied to the scalar field. In the classical limit this partition function reduces to

$$Z_S(\phi_0) = \exp(-I_S(\phi_0)) \tag{2.7}$$

where I_S is the supergravity action evaluated on the classical solution. With this dictionary, we could now compute correlation functions of the operator $\mathscr{O}$ in the large N limit by varying ϕ_0, and using the classical equations of motion in the bulk to evaluate the right-hand side. In particular, we can calculate the expectation value (the one-point function) of the boundary operator $\mathscr{O}$ in terms of the bulk scalar field ϕ. This turns out to be given by the next leading order piece in the asymptotic expansion of ϕ near the boundary. If ϕ obeys the Klein-Gordon equation with mass m, then near the boundary it can be expanded as

$$\phi(z, x^\mu) = \phi_0(x^\mu) z^{\Delta_-} + \phi_1(x^\mu) z^{\Delta_+} + \ldots \tag{2.8}$$

where

$$\Delta_\pm = \frac{d}{2} \pm \sqrt{\frac{d^2}{4} + m^2 L^2}. \tag{2.9}$$

The expectation value of $\mathcal{O}$ is then proportional to ϕ_1, as might be expected on dimensional grounds. This same pattern is repeated for all of the classical bulk fields. For each field there is a boundary condition, and this is identified with a source for some operator in the boundary theory. The expectation value of the operator is given by a sub-leading term in the asymptotic expansion of the field near the boundary (the required order of the term can be determined using dimensional analysis). Note that for scalar fields, the scaling dimension of the corresponding operator, Δ_+, depends on the scalar field mass m.

One important class of fields in the bulk are the gauge fields. Examples might include an electromagnetic vector potential associated with a $U(1)$ gauge symmetry, or the metric itself, associated with diffeomorphism invariance. Gauge fields are dynamical, but their evolution is underdetermined. There will be many distinct solutions with the same initial conditions, related by gauge transformations, since gauge transformations can vary arbitrarily in space and time. For this reason, gauge invariance is usually thought of not as a physical symmetry, but as a redundancy in our mathematical description. It is natural to ask what the significance of this bulk gauge invariance is on the boundary.

Recall that the boundary conditions we impose on our gauge fields are non-dynamical, and are identified with sources in the boundary theory. These boundary conditions will generically be altered by gauge transformations, so in a sense there is still a redundancy in our mathematical description of the boundary, but since the boundary conditions are non-dynamical this is no longer gauge invariance. The boundary dynamics are not underdetermined. However, there is a special set of gauge transformations which preserve the gauge field boundary conditions, despite acting non-trivially in the bulk. If the gauge group is G, so that a general gauge transformation is a G valued function $g(z,x^\mu)$, then this is the set of gauge transformations for which $g(0,x^\mu) = g_0$ is constant. Such transformations can mix up the boundary operators while preserving the gauge field boundary conditions, and leaving the action invariant. They can therefore be interpreted as *global* symmetries on the boundary. Another aspect of the duality has now been made precise: gauge symmetries in the bulk are dual to global symmetries of the boundary. Conversely, any global symmetry of the boundary should be gauged in the bulk, since there are no global symmetries in quantum gravity [63].

This correspondence can be made more concrete. Consider the case of a $U(1)$ symmetry. We have a bulk gauge field A^a, which we have seen should be dual to some source/operator pair on the boundary. On the other hand, we have a global $U(1)$ symmetry on the boundary which must have a corresponding conserved current operator, J^μ, and this should be dual to some bulk field. It turns out that A is dual to J. If we work in a gauge where $A^z = 0$, then the

gauge field can be expanded near the boundary as

$$A^{\mu} = A^{\mu}_{(0)} + A^{\mu}_{(1)} z^{d-2} + \ldots \tag{2.10}$$

and it can be shown that bulk gauge invariance implies $\partial_{\mu} A^{\mu}_{(1)} = 0$. For this reason we identify $A^{\mu}_{(1)}$ with $\langle J^{\mu} \rangle$. Roughly, the idea is that if we vary the bulk fields around a solution to the equations of motion, then the action can only change by a boundary term. In the special case where we apply an arbitrary infinitesimal gauge transformation, even this boundary term must vanish, since the action is gauge invariant. The gauge field variation is an exact derivative, and so applying integration by parts with respect to the boundary coordinates shows that the current $A^{\mu}_{(1)}$ is conserved. The same story holds for the metric, where in the appropriate gauge we can extract a conserved boundary stress tensor from its $O(z^{d-2})$ behaviour. The conservation of this stress tensor is a direct consequence of diffeomorphism invariance in the bulk.

Finally, we can try to understand what happens in the bulk if we place the boundary theory at some finite temperature. The concept of temperature arises in situations where we do not know the state of a system exactly, but only a probability distribution, or ensemble, to which it belongs. In classical mechanics, dealing with this uncertainty requires a lot of extra work, and the introduction of new mathematical machinery. Remarkably, in quantum field theory there is a simple recipe for adapting our description of the dynamics to obtain results at finite temperature. This is because the partition function from the path integral formulation of quantum field theory is already strikingly similar to the partition function from statistical mechanics (so similar that they are given the same name). The partition function (in the statistical sense) for a quantum mechanical system at temperature T is given by

$$Z = \sum_{n} \langle n | e^{-\hat{H}/T} | n \rangle \tag{2.11}$$

where the states $|n\rangle$ are a basis of the Hilbert space. This can be compared with the partition function (in the path integral sense) for a quantum theory on a background where the time coordinate is periodic with period τ

$$Z = \sum_{n} \langle n | e^{-i\hat{H}\tau} | n \rangle. \tag{2.12}$$

So in order to place a quantum system at temperature T, all we have to do is euclideanize time, and periodically identify the euclidean time coordinate with period $1/T$. Finite temperature correlation functions can then be obtained using the Feynman rules in the usual way.

Since the holographic dictionary identifies the time coordinate on the boundary with the time coordinate in the bulk, we should be able to obtain a gravitational description of a finite temperature CFT by applying the same recipe. We should look for stationary asymptotically AdS solutions to Einstein's equation in Euclidean signature, where the time coordinate has period $1/T$. There are only two known non-singular solutions of this type [31]: AdS itself with periodic identification, and an AdS-Schwarzschild black hole with Hawking temperature $T_H = T$. Consider first the standard case of a spherical boundary. When T is small, no black hole solution exists (spherical AdS-Schwarzschild black holes have a minimum temperature), but when T is sufficiently large the black hole solution dominates the canonical ensemble (its action is smaller than that of AdS). The phase transition between the two regimes is known as the Hawking-Page transition [31], and it is believed to be dual to a confinement transition in the CFT[7] [62]. The temperature of the phase transition is proportional to $1/L$, where L, the AdS curvature scale, is also the radius of the sphere that the boundary CFT lives on. This has to be the case, since the boundary theory is conformal, and so L is the only length scale available. If we put the same CFT on a plane, with no natural length scale, then there can be no phase transition. In this case, we find that the appropriate bulk geometry is the planar AdS-Schwarzschild black hole, which can take any temperature. In summary, at least at large T, the gravitational dual of a finite temperature holographic CFT is an AdS black hole with Hawking temperature $T_H = T$.

We have now discussed various aspects of the holographic dictionary in the limit where the bulk becomes classical. We could try to leverage these ideas to gain insight into the large N limit of strongly coupled gauge theories, but that is outside the scope of this thesis. For our purposes, the AdS/CFT correspondence is relevant for two reasons. It provides some motivation for studying gravity in asymptotically AdS space. But also, it provides a new source of intuition for thinking about gravitational problems in this regime. This will be helpful when we discuss some proposed counterexamples to cosmic censorship.

2.3.3 Restating the WCCC in AdS

In asymptotically flat space, the WCCC roughly said that if we start from good initial data, then we cannot form a singularity which is visible at $\mathscr{I}^+$. The natural generalization of this to asymptotically AdS space is to say that if we start from good initial data, and impose good boundary conditions, then we cannot form a singularity which is visible at the boundary. Just like in flat space, we will need to add some conditions to this statement in order for it to have

[7] Strictly speaking this phase transition is only present in the infinite N limit.

a chance of being true: non-generic counter-examples are allowed, the matter fields must be suitably well behaved, and the number of space-time dimensions should be $3+1$[8].

We could now attempt to give a precise formulation of the WCCC in AdS in terms of the predictability of solutions to Einstein's equation. However, the examples we consider, which we will call counter-examples to cosmic censorship, would not actually violate this precise statement. In these examples, no naked singularity forms in finite time. Instead, the curvature grows in time without bound in a region visible to the boundary. If the analogous scenario arose in asymptotically flat space, it would not violate the commonly accepted technical statement of the WCCC discussed previously, since we are still able to classically continue the evolution arbitrarily far into the future. But it does violate the *spirit* of the WCCC. Recall that the WCCC is interesting because it says that regions where we expect new physics to be important are generically hidden from view. But in our examples, whatever the curvature scale is at which new physics kicks in, such curvatures will eventually be visible to a distant observer who is prepared to wait for a sufficiently long time. It might be objected that even in flat space we can always find an open set of initial data whose evolution exceeds some given curvature bound (we could take a set of solutions near the critical value in gravitational collapse for example). But this still requires fine tuning: the higher the desired curvature, the more careful the tuning must be. What is special about our examples is that we have an open set of initial data for which the curvature during the evolution exceeds *any* bound.

We therefore propose a strengthened form of the WCCC

Conjecture 2.3.1. *For any open set of initial data (+boundary conditions) there exists a $K>0$ such that for some member of the set, $|R^{abcd}R_{abcd}|<K$ on or outside of the black hole horizons throughout the entire evolution.*

This form of the conjecture is stronger, in that it forbids large naked curvatures even if the curvature never actually becomes infinite anywhere[9], but it could be said to more accurately capture the spirit of cosmic censorship. In asymptotically flat space, its status is similar to the formulation of the WCCC in terms of predictability. All the evidence we saw in favour of the WCCC in that context can also be taken as evidence in favour of this strengthened form. But in asymptotically AdS space, we will present numerical evidence that this strengthened form of the conjecture is violated. First, we will work in vacuum where the WCCC may be violated, but things are still not completely clear. Then, we will introduce a $U(1)$ gauge field, where the evidence that the WCCC is violated is much stronger. But before we can present these solutions, we should first explain how to construct them.

[8] In higher dimensions a sufficiently small AdS-black ring solution should behave like its asymptotically flat counterpart, where the WCCC is violated.

[9] It is also weaker in that it only covers curvature singularities.

Chapter 3

Numerical Evolution with a Characteristic Scheme

Any method for constructing numerical solutions to Einstein's equation must deal with the problem of gauge invariance. Even when we specify initial and boundary conditions, Einstein's equation is underdetermined. If we have one solution then we can always apply a coordinate transformation to obtain another. If we want a well-posed set of equations, we must therefore fix a gauge by specifying which coordinate system we are going to use. This is a non-trivial problem, and if done badly the solution may become singular because the coordinate system breaks down, rather than because of any genuine pathology in the spacetime[1]. This would then prevent us from continuing the evolution any further into the future.

The solutions in this thesis have all been obtained using a characteristic scheme. This means working with coordinates corresponding to a null slicing of the spacetime. The particular null slicing is uniquely fixed because we explicitly specify the null geodesics which generate it. The advantage of such a scheme is that the set of PDEs we need to solve take on a remarkably simple form, since the coordinates have been adapted to characteristic curves of Einstein's equation (null geodesics) and most of the problem is reduced to integrating ODEs along these curves. When they work, characteristic schemes are therefore very powerful. However, it is possible that caustics will form during the evolution (where two of the null geodesics intersect) at which point the coordinate system will break down. Fortunately, we have been able to avoid this problem for the solutions we have constructed.

In this chapter we present the Bondi-Sachs coordinate system [5], which can be used to perform characteristic evolution in asymptotically flat space [61]. We then review how

[1] We can compute gauge invariant quantities such as the Kretschmann to test whether a singularity is an artefact of the choice of coordinates or not.

this coordinate system can be adapted to describe asymptotically AdS space with a finite temperature horizon, and we describe in detail a characteristic scheme which can be applied in that context [3].

3.1 The Bondi-Sachs Coordinate System

The standard way to apply a characteristic scheme in asymptotically flat space is to work in the Bondi-Sachs coordinate system, which was introduced in [5] in order to study gravitational waves. The coordinate system is constructed as follows. First, pick a timelike curve O to use as an origin (its intersection with any Cauchy surface will be a point). Then, enclose this point inside a sphere[2] on which we pick coordinates ψ, ϕ and a time coordinate v. Now consider all the null geodesics which emanate from O. These can be labelled by the coordinates of their intersection with the sphere (v, ψ, ϕ) and each can be parametrised with some parameter r. This then defines coordinates for the entire spacetime: (v, r, ψ, ϕ). For any event E we just find the null geodesic it lives on, which is labelled by some v, ψ, ϕ, and then we find the value of the parameter r on this geodesic at E. This construction works provided that this family of null geodesics does actually cover the spacetime, and provided that no two of these null geodesics ever cross (otherwise there would be an ambiguity in how this event is labelled).

Assuming that this procedure does give a valid set of coordinates for the spacetime, there is still one more potential problem. Although a constant v surface in these coordinates is made out of a family of null geodesics, this does not guarantee that the surface itself is null. It will generically be timelike in places, which is a problem if we want to treat v as the "time" coordinate in our numerics. Fortunately we still have a great deal of freedom in our specification of the coordinates: we did not say how to choose the coordinates v, ψ, ϕ on the sphere, and we did not say how to choose the parameter r along each geodesic. It is shown in [5] how the coordinate v can be chosen on the sphere to ensure that constant v surfaces are null. When this is done the metric takes the following form

$$ds^2 = -\left(Vr^{-1}e^{2\beta} - r^2 h_{AB}U^A U^B\right)dv^2 - 2e^{2\beta}dvdr - 2r^2 h_{AB}U^B dvdx^A + r^2 h_{AB}dx^A dx^B \tag{3.1}$$

where $dx^A = (d\psi, d\phi)$ and

$$h = e^{2\chi}\begin{pmatrix} e^{\alpha}\cosh\theta & \sinh\theta \\ \sinh\theta & e^{-\alpha}\cosh\theta \end{pmatrix}. \tag{3.2}$$

[2] by which we mean a surface with topology of a sphere

The only place dr appears is in the $dvdr$ term, which implies that constant v slices are null. Even in this restricted form, we still have some gauge freedom left. We have not specified how to parametrise the null geodesics, and so we can replace r with any new coordinate $\tilde{r} = \tilde{r}(v, r, \theta, \phi)$ without changing the structure of the metric. This freedom must be dealt with in any implementation of a characteristic scheme using Bondi-Sachs coordinates.

3.2 Bondi-Sachs Coordinates in AdS: A Characteristic Scheme for Asymptotically AdS Space at Finite Temperature

3.2.1 Constructing the Coordinates

The numerical scheme used in this thesis closely follows the scheme presented in [3], which we now review. The idea is to adapt the construction of Bondi-Sachs coordinates so that it can be applied in asymptotically AdS spaces with a finite temperature horizon. As before, we fill the space with null geodesics, but instead of labelling them according to their intersection with some spherical surface, we use their point of intersection with the AdS boundary. If we choose coordinates on the boundary v, x^A, x^B and introduce a parameter z along each of our null geodesics (so that $z = 0$ corresponds to the AdS boundary), then just as before we can use v, z, x^A, x^B as coordinates for the entire spacetime.

There are two problems that arise with this construction. First, there is an additional ambiguity that was not present in asymptotically flat space, because there is no analogue of the origin O. This means that the labels v, x^A, x^B do not yet uniquely specify the null geodesic. We know where it intersects the boundary, but we do not know in which direction it is pointing. Second, we again need to ensure that constant v slices will be null, but we do not now want to do this by redefining our boundary coordinate v, because we would like to specify our boundary conditions in terms of v during the setup of the problem. Fortunately, these two issues have a common solution. The new ambiguity can be fixed by requiring that constant v slices are null, and we do not then have to give up our freedom to pick the boundary coordinates however we like.

It might not be immediately obvious how this works. We have a two parameter family of null directions to choose from at each point on the boundary, and only a single constraint: the normal to the generated surface should square to zero. But in fact, this single constraint fixes both degrees of freedom. There are two independent spacelike vectors which lie in a constant v surface at any point on the boundary, and the two dimensional space of covectors orthogonal to these contains only a single null direction, $\hat{n}_a$. We are therefore forced to

choose our geodesic so that $\hat{n}_a$ ends up being the normal to our constant v surface in the bulk. The only way to do this is to pick the geodesic with tangent $\hat{n}^a$.

So the end result of this discussion is that we are led to the metric ansatz presented in [3]:

$$ds^2 = -\left(e^{2\beta}Vz - \frac{h_{AB}U^AU^B}{z^2}\right)dv^2 - \frac{2e^{2\beta}}{z^2}dvdz - \frac{2h_{AB}U^B}{z^2}dvdx^A + \frac{h_{AB}}{z^2}dx^Adx^B \quad (3.3)$$

where again

$$h = e^{2\chi}\begin{pmatrix} e^{\alpha}\cosh\theta & \sinh\theta \\ \sinh\theta & e^{-\alpha}\cosh\theta \end{pmatrix}. \quad (3.4)$$

The metric in this form still has the remaining gauge freedom corresponding to redefinitions of the bulk radial coordinate z, and this can be used to fix the function χ. In [3] they fix the z dependence of χ to be of the form

$$\chi(v,z,x^A,x^B) = \frac{1}{4}\log(1+2z^3\chi_3(v,x^A,x^B)) \quad (3.5)$$

but there is still some gauge freedom left, as χ_3 is unspecified. In particular, although we can specify the initial value of χ_3 as part of our initial conditions, $\dot{\chi}_3$ will not be determined by the equations of motion (where $\dot{}$ denotes a derivative with respect to v). This freedom is used to choose $\dot{\chi}_3$ during the evolution so that the apparent horizon remains fixed at $z=1$, which will be the inner boundary of our computational domain. The apparent horizon is expected to always lie inside the event horizon, so by imposing this condition we should guarantee that the entire exterior of the black hole region is being captured. In order to impose this apparent horizon condition, we will need an explicit expression for the expansion of a set of null geodesics orthogonal to the $z=1$ surface. An apparent horizon is a surface for which this expansion vanishes, so we want to be able to pick $\dot{\chi}_3$ to ensure that this happens.

3.2.2 The Apparent Horizon Condition

Consider a congruence of null geodesics with tangent ξ^μ. This vector field must then obey the conditions $\xi^\mu\xi_\mu = 0$ and $\xi^\mu\xi_{\rho;\mu} = 0$. The expansion of the null geodesic congruence is given by $\xi^\mu{}_{;\mu}$. We are interested in the outgoing null geodesics which are orthogonal to the $z=1$ surface at a particular time v_0. Construct a function $S[v_0](v,z,x^A,x^B)$ such that the surface generated by these null geodesics corresponds to $S=0$. The tangents to the null geodesics are orthogonal to themselves, and to the $z=1, v=v_0$ surface, so when we lower their index we must get something proportional to the normal to S : $\xi_\mu = RS_{,\mu}$. We are free to pick the 3 parameter function $S[v_0](v_0,z,x^A,x^B)$ however we like provided that it vanishes

on $z=1$, and this gives us most of the partial derivatives of S. The conditions $\xi^\mu \xi_\mu = 0$ and $\xi^\mu \xi_{\rho;\mu} = 0$ can then be used to solve for $S_{,v}$ and $R_{,v}$. This turns out to be enough to show that the expansion on $z=1$, given by $\xi^\mu{}_{;\mu}$, is proportional to

$$z^2(z\partial_z\chi - 1)V - D_A U^A - 2\dot{\chi}|_{z=1} \tag{3.6}$$

where the symbol D_A denotes the covariant derivative with respect to the 2 dimensional metric h_{AB}. It will be convenient to introduce a new function

$$d_t\chi \equiv \dot{\chi} - \frac{z^2}{2}(z\partial_z\chi - 1)V \tag{3.7}$$

and the apparent horizon condition can then be written

$$d_t\chi + \frac{1}{2}D_A U^A|_{z=1} = 0. \tag{3.8}$$

3.2.3 The Numerical Scheme

We are now ready to present the details of the numerical scheme. The basic idea is to show how the functions $\beta, U^A, V, \dot{\alpha}, \dot{\theta}$ and $\dot{\chi}$ can be determined on a given time slice if the functions α, θ and χ are known. We can then use the time derivatives to jump to the next time slice, and repeat the same procedure again. There is an additional complication, because it turns out that we will also need to assume some knowledge of the boundary behaviour of U^A and V beyond what is given to us by the boundary conditions. In holographic language, we need to know some components of the boundary stress tensor. However, the time derivatives of these components can also be determined, so we can evolve them between time slices in the same way that we evolve α, θ and χ.

The first step of the scheme is to solve the zz component of Einstein's equation for β :

$$\frac{4}{z}(-1 + z\partial_z\chi)\partial_z\beta - 2\partial_z^2\chi - \frac{1}{2}\left(4(\partial_z\chi)^2 + (\partial_z\alpha)^2\cosh^2\theta + (\partial_z\theta)^2\right) = 0. \tag{3.9}$$

Next, we define an auxiliary function

$$\pi^A \equiv z^{-2}e^{2(\chi-\beta)}h_{AB}\partial_z U^B \tag{3.10}$$

and this function can then be solved for using the Az component:

$$\frac{z^2e^{-2\chi}}{2}\partial_z\pi_A - \frac{1}{z^2}e^{2\chi}\partial_z(z^2e^{-2\chi}\partial_A\beta) + \frac{1}{2}h^{BC}D_C\partial_z h_{AB} - 2D_A\partial_z\chi = 0. \tag{3.11}$$

To solve this equation, we need boundary data for π^A, but this is not given to us by the AdS boundary conditions. This is the first step where some knowledge of the boundary stress tensor is required. We will therefore need to ensure that we can propagate boundary data for π^A between time slices so that this equation can be solved. Once we have π^A, it is then straightforward to determine U^A by inverting Equation 3.10.

With β and U^A determined, it remains to solve for $V, \dot{\alpha}, \dot{\theta}$ and $\dot{\chi}$. Instead of solving for V directly, the next step is to solve for the function we introduced in Equation 3.7: $d_t\chi$. This can be done using the combination

$$h^{AB}G_{AB} = 4e^{-2(\beta+\chi)}z^2\partial_z\left(\frac{e^{2\chi}}{z^2}d_t\chi\right) - \frac{1}{2}e^{-4\beta}h_{AB}\partial_z U^A\partial_z U^B - \frac{2\Lambda}{z^2} + \mathscr{R} - 2e^{-\beta-2\chi}D_A e^{2\chi}h^{AB}D_B e^{\beta} + z^4 e^{-2(\beta+\chi)}D_A e^{-2\chi}\partial_z\left(\frac{e^{4\chi}U^A}{z^4}\right) = 0 \quad (3.12)$$

where $\mathscr{R}$ is the Ricci scalar associated with the metric h_{AB}. In principle, we again require some knowledge of the boundary stress tensor here to provide the necessary boundary data for $d_t\chi$ (we need to know its behaviour at $O(z^2)$). This is another piece of boundary data which should be dynamically evolved between time slices. However, since we know that we are going to eventually choose $\dot{\chi}$ in order to enforce the apparent horizon condition, we could actually use the apparent horizon condition itself here (given in Equation 3.8) as a boundary condition for $d_t\chi$ at $z = 1$. If our scheme is consistent, then both of these approaches should give the same answer, which gives us a way of monitoring the numerical error. In our solutions, we choose to evolve boundary data for $d_t\chi$ so that we can impose a boundary condition at $z = 0$, and we evaluate the left hand side of Equation 3.8 at $z = 1$ to monitor the numerical error.

It turns out that although we still do not know V, we can now use the two remaining linearly independent combinations of G_{AB} to solve for the two auxiliary functions

$$d_t\alpha \equiv \dot{\alpha} - \frac{z^3}{2}V\partial_z\alpha \quad (3.13)$$

$$d_t\theta \equiv \dot{\theta} - \frac{z^3}{2}V\partial_z\theta. \quad (3.14)$$

This requires us to solve two coupled linear equations simultaneously.

Apart from the time derivatives of our boundary data, the only functions left to determine are now $\dot{\chi}$ and V, and since these are now related by Equation 3.7, there is really only one unknown function remaining. In principle, we should be able to freely specify $\dot{\chi}$ at this point due to the remaining gauge freedom, but recall that we would like to choose it to ensure that

the apparent horizon condition is enforced. Imposing this condition directly is not possible, because we have seen that the expansion, given by the left hand side of Equation 3.8, should already have been determined when we solved for $d_t\chi$. However, it turns out that we can make sure that its *time derivative* vanishes. That way, we just need the apparent horizon to lie at $z=1$ in our initial data, and it will remain there for all times.

In order to do this, we consider the combination $G^z{}_t + U^A G^z{}_A$. If we suppose that the time derivative of the left hand side of Equation 3.8 vanishes, and also make use of Equation 3.9, then this reduces to an elliptic equation for V at $z=1$:

$$-\frac{1}{2}D^2V - \frac{1}{2}\left(e^{-2\beta}\partial_z U + 2D\beta\right)\cdot DV - \left(\partial_z d_t\chi + \frac{1}{2}D\cdot U - U\cdot D\partial_z\chi\right)e^{-2\beta}V$$
$$+ e^{-2(\beta-\chi)}d_t\left(e^{-2\chi}h_{AB}\right)D^AU^B + \frac{1}{4}e^{-2(\beta-2\chi)}d_t\left(e^{-2\chi}h_{AB}\right)d_t\left(e^{-2\chi}h^{AB}\right)$$
$$+ \frac{1}{2}e^{-2\beta}\left((D_AU^B)(D^AU_B) + (D_AU^B)(D_BU^A) - (D\cdot U)^2\right)|_{z=1} = 0. \quad (3.15)$$

This can be solved to determine V on $z=1$, and that then determines $\dot{\chi}$ through Equation 3.7. But the z dependence of $\dot{\chi}$ was fixed in Equation 3.5, so the fact that we know its value on $z=1$ allows us to compute it (and V via Equation 3.7 again) everywhere.

All that remains to do is explain how to evolve the boundary data for π^A and $d_t\chi$. Since we now have most of the solution on the time slice (we already know $\chi,\alpha,\theta,\beta,U^A,V,\dot{\chi},\dot{\alpha}$ and $\dot{\theta}$), extracting the time derivatives of the boundary data from the remaining equations of motion turns out to be relatively straightforward. If we expand the *vA* component of Einstein's equation near the boundary, this can be rearranged to give an expression for $\dot{\pi}_3|_{z=0}$ (no integration is required). Similarly, the *vv* equation at the boundary gives $\frac{\partial_v d_t\chi}{z^2}|_{z=0}$. These are precisely the quantities we need to evolve the boundary data forward. Roughly, this corresponds to evolving the momentum density and energy density of the boundary stress tensor. The equations we use to do this are equivalent to enforcing conservation of this stress tensor[3].

3.2.4 Boundary Conditions

We have now explained the order in which the equations must be solved. We have also claimed that some necessary boundary data is not determined by the boundary conditions, and must therefore be evolved between time slices, and we have explained how this can be

[3]The remaining 2 independent components of this stress tensor are related to the behaviour of α and θ near the boundary, which we also evolve between adjacent time slices.

done. However, we have not yet been explicit about what the boundary conditions themselves actually are, or about how our metric functions behave near the boundary.

The boundary conditions we must provide correspond to fixing the $O(1/z^2)$ behaviour of the metric near $z = 0$. In holographic language, we must fix the boundary metric, and typically we impose that the boundary metric is flat[4]. When this is done, we find the following expansions near $z = 0$:

$$V = \frac{1}{z^3} + V_3 + O(z) \tag{3.16}$$

$$\beta = -\frac{1}{2}\chi_3 z^3 + O(z^4) \tag{3.17}$$

$$U^A = U_3^A z^3 + O(z^4) \tag{3.18}$$

$$\alpha = \alpha_3 z^3 + O(z^4) \tag{3.19}$$

$$\theta = \theta_3 z^3 + O(z^4). \tag{3.20}$$

The five integration constants $V_3, \alpha_3, \theta_3, U_3^A$ describe the five degrees of freedom of the traceless boundary stress tensor.

Sometimes, we will want to deform the boundary metric, and in this case the expansions of the metric functions off the boundary become more complicated. For the problems considered in this thesis, we typically impose non-trivial boundary conditions on the functions U^A. In this case we find the following expansions

$$V = \frac{1}{z^3} - \partial_A U_0^A \frac{1}{z^2} - \frac{3}{8}\left(\delta_{AB}\delta^{CD}\partial_C U_0^A \partial_D U_0^B + \partial_A U_0^B \partial_B U_0^A - \partial_A U_0^A \partial_B U_0^B\right)\frac{1}{z} + V_3 + O(z) \tag{3.21}$$

$$\beta = -\frac{1}{16}\left(\delta_{AB}\delta^{CD}\partial_C U_0^A \partial_D U_0^B + \partial_A U_0^B \partial_B U_0^A - \partial_A U_0^A \partial_B U_0^B\right) z^2 - \frac{1}{2}\chi_3 z^3 + O(z^4) \tag{3.22}$$

$$U^A = U_0^A + \frac{1}{2}\delta^{BC}\partial_B\partial_C U_0^A z^2 + U_3^A z^3 + O(z^4) \tag{3.23}$$

$$\alpha = \left(\partial_1 U_0^1 - \partial_2 U_0^2\right) z + \alpha_3 z^3 + O(z^4) \tag{3.24}$$

$$\sinh\theta = \left(\partial_2 U_0^1 + \partial_1 U_0^2\right) z + \theta_3 z^3 + O(z^4) \tag{3.25}$$

where the source term U_0^A is some function of the boundary coordinates.

[4]When we include an electromagnetic field together with this boundary condition it does not affect the given expansions.

3.2.5 Conclusion

This completes the description of the characteristic scheme for finite temperature asymptotically AdS space. To actually implement this scheme in practice we will need to pick a numerical method for solving the ODEs along each characteristic, for solving the elliptic equation for V on $z = 1$, and for performing the time evolution. We have used spectral methods to do the first two of these, with a Chebyshev grid in the z direction, and either a Fourier or Chebyshev grid in the boundary directions according to whether they are periodic or not. To perform the time evolution, we use the 4th order Runge-Kutta method. We also apply filtering every few time steps to improve numerical stability. This means interpolating onto a smaller grid (with about $2/3$ the number of grid points) and back again, which helps to reduce the effects of aliasing error.

Chapter 4

Refining the Characteristic Scheme: Gauge fields, Zero Temperature, and Non-Compact Boundaries

The characteristic scheme from [3], presented in the previous chapter, allows us to solve time dependent problems in asymptotically AdS spaces in vacuum at finite temperature, and it works well when the boundary coordinates are all compact. However, many of the problems that we are going to consider will not satisfy all of these conditions. First, we will sometimes want to include an electromagnetic field. This will require us to add a few more steps to the scheme, involving the electromagnetic field and its equation of motion. We present these new steps in the first half of this chapter. Second, we will sometimes want to work at zero temperature. It is more difficult to see how the scheme should be adapted to cope in this context. In the second half of this chapter, we explain how it can be done by presenting a new way of constructing the coordinates. To our knowledge, this is the first time that time evolution has been performed in an asymptotically AdS space-time with a planar zero temperature horizon. Finally, we will sometimes want to consider cases where the boundary coordinates are non-compact. Although it is not immediately obvious that the previous scheme will fail to cope with a non-compact boundary, we have not been able to make it work. We explain why at the end of this chapter, and why the adaptations that we make to the scheme to handle zero temperature can solve this problem as well.

4.1 Introducing an Electromagnetic Field

The Einstein-Maxwell action is

$$S = \frac{1}{16\pi}\int d^4x\sqrt{-g}\left(R + \frac{6}{L^2} - F_{ab}F^{ab}\right) \tag{4.1}$$

where

$$F = dA. \tag{4.2}$$

The vector potential A comes with its own gauge freedom that must be fixed before we can apply a numerical scheme. In particular, for any function ψ, we can add $d\psi$ to A to obtain another solution to the equations of motion, since this transformation leaves F invariant. We choose to fix this freedom by imposing that $A_z = 0$. Given an arbitrary gauge field configuration, we can always achieve this condition by choosing ψ such that $\partial_z\psi = -A_z$, as this equation can be solved by integrating inwards from the boundary. The solution will be unique (up to a constant) since if ψ had any dependence on the boundary coordinates at $z = 0$ then this would affect the boundary conditions. There is therefore no more gauge freedom left. Additionally, in all of the problems we consider with a gauge field, there will always be a symmetry under the reflection or translation of one of the boundary coordinates, so this leaves only 2 non-zero components:

$$A(v,z,x) = A_v(v,z,x)dv + A_x(v,z,x)dx \tag{4.3}$$

where x is the single boundary coordinate on which our functions can depend.

The introduction of this gauge field will alter all of the equations that we had previously, because there is now a non-zero stress tensor on the right hand side of Einstein's equation. Fortunately, this turns out to not disrupt the scheme too much. We just need to add A_x to the list of fields that we assume we know, and then we have to add steps to the scheme to solve for A_v and $\dot{A}_x$ at the appropriate places. The right hand side of the new version of equation 3.9 (coming from T_{zz}) depends only on A_x, not on A_v, so we can solve for β again straight away. Next, we solve for U^x and A_v together. Along with the auxiliary function π^x from Equation 3.10, we define an additional auxiliary function

$$\pi_M = e^{2\chi-2\beta}\left(\partial_z A_v + U^x\partial_z A_x\right) \tag{4.4}$$

and with this definition, the v component of Maxwell's equation $\nabla_\mu F^{\mu\nu} = 0$, reduces to

$$e^{\alpha}\partial_z\pi_M - \partial_x\partial_z A_x + (\partial_x\alpha)(\partial_z A_x) = 0 \tag{4.5}$$

which we can solve for π_M. Just like with π^x, solving this equation requires more boundary data than is given to us by the boundary conditions. In holographic language, this is the boundary data associated with the charge density under the global $U(1)$ symmetry on the boundary. Just like with the components of the boundary stress tensor, we will later have to evolve this boundary data between time slices. For now though, with π_M determined, we can solve the new version of Equation 3.11 for π^x, since the new right hand side (coming from T_{xz}) can be written in terms of π_M. We can then determine U^x and A_v by inverting Equation 3.10 and 4.4 in that order.

The next step is to find $d_t\chi$, which we were able to do in the original scheme by solving $h^{AB}G_{AB} = 0$. The right hand side of this equation is now non-zero, but it turns out that we can evaluate it using the functions we have found so far. This means we can solve the new equation for $d_t\chi$ in the same way. We are then supposed to solve for $d_t\alpha$ and $d_t\theta$ using the remaining two independent combinations of G_{AB}. Since we are now assuming a symmetry in one of our boundary directions, we know that $\theta = 0$, and there is only 1 independent component of G_{AB} left. This makes things easier, but we also have an additional unknown quantity to solve for: $\dot{A}_x$. It again helps to define a new quantity

$$d_t A_x = \dot{A}_x - \frac{z^3}{2} V \partial_z A_x. \tag{4.6}$$

We can then solve for $d_t\alpha$ and $d_t A_x$ together using the yy component of Einstein's equation and the x component of Maxwell's (where we use y to denote the coordinate along the symmetry direction).

With these functions all determined, we can solve for V and $\dot{\chi}$ using the same equation on the horizon as before (now with a non-zero right hand side), and all that remains is to evolve the boundary data. The vv and vA components of Einstein's equation can again be used to find the time derivatives of the boundary data for π^x and $d_t\chi$, and this is equivalent to enforcing conservation of the boundary stress tensor. But we now also need to know $\dot{\pi}_M|_{z=0}$. This can be obtained by rearranging the z component of Maxwell's equation, expanded near the boundary, and this is equivalent to enforcing charge conservation.

4.2 Zero Temperature

To understand why the previous scheme cannot cope with a vanishing temperature, and to motivate the new coordinate construction which can, it is helpful to consider pure AdS as an example. We gave the metric for the Poincaré patch of AdS in Equation 2.3, where we explained how it can be thought of as a zero temperature planar black hole. The problem

with applying the null slicing procedure of Section 3.2.1 to the Poincaré patch in the natural way is that caustics will then appear on the Poincaré horizon, as we now demonstrate.

First, let us try to explicitly construct a coordinate transformation which removes the coordinate singularity at the Poincaré horizon, $z = \infty$. There are two obvious problems contributing to the singular behaviour there: the coordinate z itself blows up, and it is a horizon. We can try to solve the first problem by replacing z with $r = L^2 z^{-1}$ and we can try to solve the second by switching to ingoing null coordinates $v = t - z$. This gives

$$ds^2 = -\frac{r^2}{L^2}dv^2 + 2dvdr + \frac{r^2}{L^2}\delta_{ij}dx^i dx^j \tag{4.7}$$

but this metric is still singular at the Poincaré horizon! All of the components of the metric in the x^i directions vanish at $r = 0$. To get rid of the coordinate singularity, we will have to do something with the x^i coordinates as well. One coordinate system that does the job, used in [35], is the following: we first transform the boundary coordinates amongst themselves to get polar coordinates on the boundary

$$ds^2|_\partial = -dt^2 + dR^2 + R^2 d\phi^2 \tag{4.8}$$

and then we define new coordinates for the bulk as follows

$$\rho^{-1} = L^{-2}\sqrt{z^2 + R^2} \tag{4.9}$$

$$\psi = \arctan\frac{z}{R} \tag{4.10}$$

$$v = t - L^2\rho^{-1}. \tag{4.11}$$

In these coordinates, the bulk metric is

$$ds^2 = \frac{1}{\sin^2\psi}\left(-\frac{\rho^2}{L^2}dv^2 + 2dvd\rho + L^2\left(d\psi^2 + \cos^2\psi d\phi^2\right)\right) \tag{4.12}$$

which is now non-singular at the Poincaré horizon, $\rho = 0$.

We are now in a position to understand why taking the null slicing of the Poincaré patch in the natural way does not work. If we pick a time coordinate on the boundary so that the boundary metric is Minkowski, and then construct a null slicing according to the procedure described in Section 3.2.1, we will end up with something like the metric of Equation 4.7 (up to redefinitions of r). The null geodesics generating this null slicing, written in terms of the standard Poincaré patch coordinates, are of the form $t = z + c$, with the coordinates x^i constant along each geodesic. But we can now see that all of these null geodesics actually

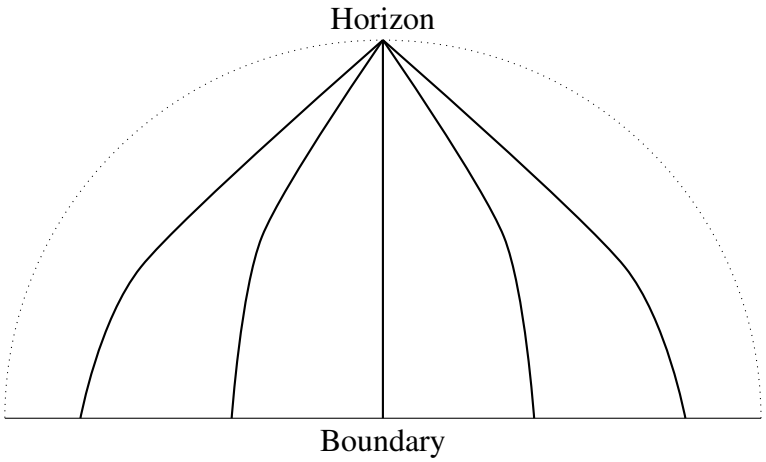

Fig. 4.1 A visualization of the null geodesics which generate the null slicing of Equation 4.7. There is a caustic on the Poincaré horizon at $\psi = \frac{\pi}{2}$.

intersect the Poincaré horizon in the same place: $\psi = \frac{\pi}{2}$. In other words, we have a caustic on the Poincaré horizon. This is why the metric in Equation 4.7 is singular there. The null geodesics are shown pictorially in Figure 4.1.

We have also seen that a non-singular null slicing *is* possible. An example of such a slicing is provided by the coordinates we used to construct the metric 4.12. The null geodesics generating this null slicing are visualised in Figure 4.2. But although these null geodesics cover the entire horizon, they do not cover the whole boundary. They only intersect the origin, $R = 0$. This is a problem if we want to formulate a numerical scheme in the way we outlined in Section 3.2. In particular, it is not true that every point on the boundary has a unique v, ψ, and ϕ coordinate.

How should we proceed? The idea is to pick a null slicing which is a compromise between Figure 4.1 and Figure 4.2. We want to fill the space with null geodesics so that they cover the whole boundary *and* the whole horizon. This is depicted pictorially in Figure 4.3. We can do this in pure AdS by constructing coordinates in the following way:

$$\rho^{-1} = L^{-2}\sqrt{(z+c)^2 + R^2} \tag{4.13}$$

$$\psi = \arctan\frac{z+c}{R} \tag{4.14}$$

$$v = t - L^2\rho^{-1} \tag{4.15}$$

for some arbitrary constant c (we always work with $c = 1$). This puts the metric in the form

$$ds^2 = \frac{1}{(\sin\psi - c\rho/L^2)^2}\left(-\frac{\rho^2}{L^2}dv^2 + 2dvd\rho + L^2(d\psi^2 + \cos^2\psi d\phi^2)\right). \tag{4.16}$$

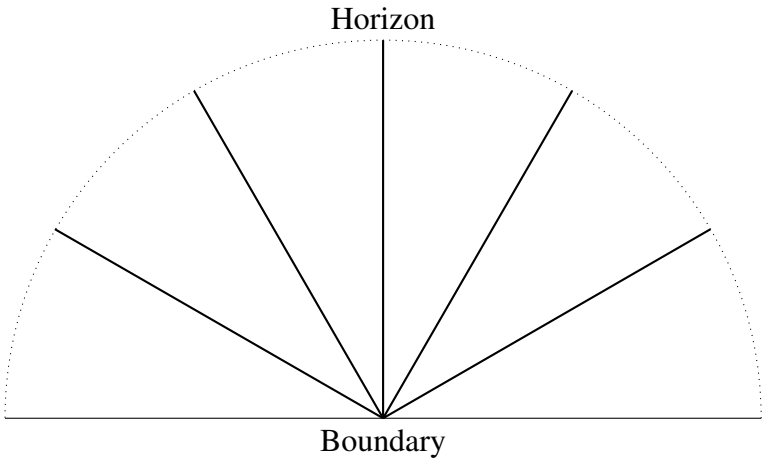

Fig. 4.2 A visualization of the null geodesics which generate the null slicing of Equation 4.12. There is no longer a caustic on the Poincaré horizon but now the geodesics all intersect the boundary at a single point.

For our numerics, we make the further coordinate redefinition $x = \sin\psi$ so that the metric becomes:

$$ds^2 = \frac{1}{(x-c\rho/L^2)^2}\left(-\frac{\rho^2}{L^2}dv^2 + 2dvd\rho + L^2\left(\frac{dx^2}{1-x^2} + (1-x^2)d\phi^2\right)\right). \tag{4.17}$$

This metric is non-singular at the Poincaré horizon $\rho = 0$, but at the same time, v, x and ϕ can still be used as coordinates on the boundary. When this is done, the boundary metric (still flat) takes the unusual form

$$ds^2|_\partial = -dv^2 + 2\frac{c}{x^2}dvdx + \frac{c^2}{x^2}\left(\frac{dx^2}{1-x^2} + (1-x^2)d\phi^2\right). \tag{4.18}$$

So in a general asymptotically AdS space-time, if we choose these coordinates on the boundary, and apply the recipe of Section 3.2.1 to construct a null slicing for our numerical scheme, we should have a good chance of avoiding caustics on or outside of the horizon. This motivates adopting a metric ansatz

$$ds^2 = \frac{1}{(x-c\rho/L^2)^2}\left(-(e^{2\beta}V - h_{AB}U^AU^B)dv^2 + 2e^{2\beta}dvd\rho - 2h_{AB}U^Bdvdx^A + h_{AB}dx^Adx^B\right) \tag{4.19}$$

where $dx^A = (x, \phi)$ and the boundary conditions can be chosen so that the boundary metric takes the form in Equation 4.18 (note that V is defined slightly differently to the previous scheme so that it does not diverge at the boundary). With this, we can solve time dependent problems in asymptotically AdS space at zero temperature.

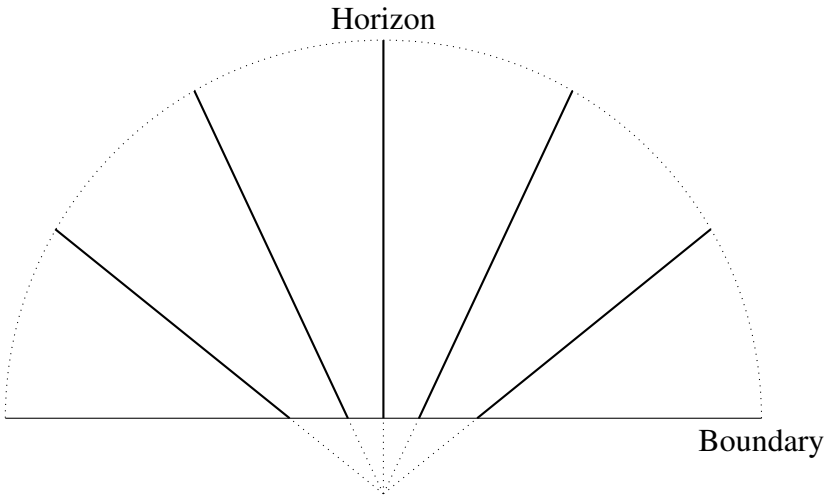

Fig. 4.3 A visualization of the null geodesics which generate the null slicing of Equation 4.17. The geodesics now cover the entire horizon *and* the entire boundary.

4.2.1 Details of the Zero Temperature Numerical Scheme

Fortunately, we can solve the equations of motion arising from this metric ansatz with a numerical scheme that is almost identical to the one that we had previously. All of the functions are solved for in the same order, using the same components of Einstein's (or Maxwell's) equation at each step. The only differences are that we need to change the way that we fix the ρ dependence of χ, and we need to give new definitions of $\pi_A, d_t\chi, d_t\alpha$, and d_tA_x. The simplest way to do this is the following. To keep χ in a similar form to before, we impose

$$\chi(v,\rho,x) = \frac{1}{4}\log\left(1+2\left(1-\frac{c\rho/L^2}{X}\right)\chi_3(v,x)\right). \tag{4.20}$$

The new definition of π_A is

$$\pi_A \equiv (x-c\rho/L^2)^{-2}e^{2(\chi-\beta)}h_{AB}\partial_z U^B \tag{4.21}$$

and the new $d_t\chi$ is

$$d_t\chi \equiv \dot{\chi} + \left(\frac{c/L^2+(x-c\rho/L^2)\partial_z\chi}{2(x-c\rho/L^2)}\right)V. \tag{4.22}$$

With this definition of $d_t\chi$ the apparent horizon condition is again

$$d_t\chi + \frac{1}{2}D_A U^A|_{\rho=0} = 0 \tag{4.23}$$

which, after we have solved for $d_t\chi$, has no dependence on $\dot{\chi}$ or V. This means that the story we had before applies here as well. We cannot impose the apparent horizon condition directly through our choice of $\dot{\chi}$, we must do it indirectly (we impose that the time derivative of the apparent horizon condition vanishes and use this to derive an elliptic equation for V on the horizon). Because we do this, we could even choose to use the apparent horizon condition as a boundary condition for $d_t\chi$ at the horizon, instead of evolving data for it at the boundary, and if our scheme is consistent then these two approaches should give the same answer. We can use this to monitor the numerical error. For the other functions beginning with d_t, we just replace $d_t = \frac{\partial}{\partial v} - \frac{z^3}{2}V\partial_z$ with $d_t = \frac{\partial}{\partial v} - \frac{1}{2}V\partial_z$.

Finally, when numerically solving the equations we need to take account of the fact that the boundary no longer lies at a constant value of ρ. Instead, it is given by $\rho = xL^2/c$. To deal with this, we make a further coordinate transformation. We use the coordinates (v,ρ,x,ϕ) to construct the metric and derive the equations of motion, but just before solving the equations numerically, we define

$$Z = 1 - \frac{c\rho}{L^2 x} \tag{4.24}$$

$$X = \sqrt{1-x}. \tag{4.25}$$

The boundary then lies at $Z = 0$, the horizon lies at $Z = 1$, and the symmetry axis lies at $X = 0$. This does not spoil the structure of the numerical scheme because

$$\frac{\partial}{\partial\rho}|_{x,\phi} = (-\frac{c}{L^2 x})\frac{\partial}{\partial Z}|_{X,\phi} \tag{4.26}$$

so if an equation contained only ρ derivatives of a given function before, it still contains only Z derivatives after. We can then solve the equations using spectral methods by introducing a Chebyshev grid in both the Z and X directions.

The definition of X ensures that if we expand any of the functions around the symmetry axis, they will contain only even powers of X. This means we can use a "doubling trick" in this direction. Although the computational domain of X is the interval $[0,1]$, we construct a Chebyshev grid on the artificially extended domain $[-1,1]$, and impose a symmetry on all of our functions under reflection through the origin. This symmetry means that we can then restrict back down to the interval $[0,1]$ and construct differentiation matrices for this half of the Chebyshev grid alone.

4.2.2 Boundary Conditions at Zero Temperature

In the previous section we gave the boundary conditions that need to be imposed on the metric functions in order to get a flat boundary metric. With these boundary conditions, the expansions of the metric functions near the boundary take a similar form to the previous Chapter. But we still need to explain how to impose non-trivial boundary conditions on the gauge field in these new coordinates, and how to deform the boundary metric if we do not want it to be flat. First, consider the gauge field. To work out how to impose boundary conditions, it is helpful to work with the gauge invariant quantity F_{ab}, rather than A_a. There is then no need to worry about how to make the $A_\rho = 0$ gauge choice.

Consider placing the field F_{ab} in an AdS background space-time, and writing it in terms of the coordinates (t, z, R, ϕ) from the previous section

$$F = F_{tR}(dt \wedge dR) + F_{tz}(dt \wedge dz) + F_{zR}(dz \wedge dR). \tag{4.27}$$

If we were to evolve the field in this background, then we would need to specify the value of F_{tR} at $z = 0$ as a boundary condition. Physically, this is the R component of the electric field at the boundary. The values of the other two functions at the boundary (the z component of the electric field and the ϕ component of the magnetic field) are fixed by Maxwell's equations. The question we need to answer then is the following. How can we write the boundary electric field, F_{tR}, in terms of the components of F in the new coordinates (v, ρ, x)? This is the expression whose value we will need to fix as a boundary condition. Performing the coordinate transformation gives the result

$$F_{tR} = -\frac{\rho x}{L^2}\sqrt{1-x^2}\left(F_{vx} + \frac{\rho}{x}F_{v\rho}\right). \tag{4.28}$$

On the boundary, we have $\rho = xL^2/c$, so this reduces to

$$F_{tR} = -\frac{x^2}{c}\sqrt{1-x^2}\left(F_{vx} + \frac{L^2}{c}F_{v\rho}\right). \tag{4.29}$$

This is the boundary condition that must be imposed. To do this, we work exclusively with F rather than A in the numerical scheme. This is easy to do, since A only appears in combinations corresponding to components of F. Then, at the step where we solve for $d_t A_x$ we pick our boundary condition on $d_t A_x$ to ensure that Equation 4.29 is satisfied.

Sometimes, rather than introducing a boundary electric field to drive the dynamics, we will want to deform the boundary metric instead. In particular, we will want to introduce $dtd\phi$ and $dRd\phi$ cross terms into the boundary metric. This again requires us to consider

how the boundary conditions will transform to the new coordinates. But there is a trick we can use to simplify this calculation. Instead of working with the functions U^ϕ and θ from before (which are the functions that would acquire non-trivial boundary conditions in this problem), we leave these out of our metric ansatz. In their place, we introduce new functions A_v and A_x and replace $d\phi$ in the metric with $(d\phi + A_v dv + A_x dx)$. Note that redefinitions of the coordinate ϕ change A by an exact derivative, so it behaves under gauge transformations like an electromagnetic field. In fact, we can then solve this problem as if it were an electromagnetic field with fixed boundary metric, with the $\phi\mu$ component of Einstein's equation playing the role of the μ component of Maxwell's (with index down). Working with F instead of A means we can then use Equation 4.29 to impose the appropriate boundary condition, just as before. One additional complication is that A now appears explicitly in some of the equations, instead of always appearing as components of F. We can fix this by replacing some of the equations of motion we use during the numerical scheme with gauge invariant combinations. The necessary replacements are as follows:

$$G_{x\phi} \to G_{x\phi} - A_x G_{\phi\phi} \tag{4.30}$$

$$G_{v\phi} \to G_{v\phi} - A_v G_{\phi\phi} \tag{4.31}$$

$$G_{vx} \to G_{vx} - A_x G_{v\phi} - A_v G_{x\phi} + A_v A_x G_{\phi\phi} \tag{4.32}$$

$$G_{vv} \to G_{vv} + A_v^2 G_{\phi\phi} - 2A_v G_{v\phi}. \tag{4.33}$$

4.2.3 Conclusion

It is interesting to ask whether this coordinate construction is the only way to perform numerical time evolution with a zero temperature planar horizon. If we want to use a characteristic scheme, then it seems likely that the answer is yes. The null geodesics we have chosen to generate our coordinates with appear to be the simplest family with the property that every point on the boundary, and on the horizon, lies on a unique geodesic. It is essential that we have this property in order for a characteristic scheme to be applicable. We do still have freedom in our choice of the parameter c, and although it has always been set to 1 for the results appearing in this thesis, it would be interesting to investigate further how different choices of this parameter affect numerical stability.

4.3 Non-Compact Boundary

In the previous section, we described a numerical scheme that works at zero temperature when the boundary directions are non-compact. Interestingly, the simpler finite temperature

numerical scheme is unable to cope with a non-compact boundary. Our attempts to use it in this context resulted in numerically unstable solutions with a boundary energy density that rapidly diverged. It is possible to understand this behaviour, and why the zero temperature scheme avoids this problem, by considering how energy conservation is enforced.

Suppose we have a boundary coordinate R which ranges from 0 to ∞. To model this on a computer, we need to apply a coordinate transformation so that the computational domain is finite. For example, we might define $R = \frac{r}{1-r^2}$ so that r ranges between 0 and 1. Now in the usual finite temperature numerical scheme, if we take the limit $R \to \infty$ on the boundary at a fixed value of v, we end up at spatial infinity of the boundary. The total energy on a constant v slice (obtained by integrating the energy density of the conserved boundary stress tensor) should therefore be constant in time. But as energy flows out towards $r = 1$, keeping track of energy conservation requires extremely precise tuning of the energy density. This is because small changes in the energy density near $r = 1$ will result in very large changes in the total energy. Numerical error therefore leads to large violations of energy conservation. This extra energy can then flow back towards smaller values of r, where it causes the energy density to diverge, making the numerical solution unstable.

The zero temperature numerical scheme avoids this problem, because now if we take the limit $R \to \infty$ with v fixed, we reach *null* infinity on the boundary. This means that as v increases, energy can be radiated away, so the total energy is no longer conserved. If small numerical errors arise in the energy density near $R = \infty$, this can still lead to a much larger error in the total energy, but the propagation of this energy back towards smaller values of R is strongly suppressed. The numerical evolution remains stable. The motivation for constructing the numerical scheme of the previous section was to handle situations with zero temperature, but it turns out that in doing this, we have also found a way to solve the problem of a non-compact boundary as well.

Chapter 5

Attempting to Form Naked Singularities in Vacuum

5.1 Motivation

In this chapter, we explain how it *may* be possible to form a naked singularity in asymptotically AdS space with no matter fields present, by imposing sufficiently violent boundary conditions on the metric [14]. As motivation, we can ask the following question: is it possible to use the AdS boundary conditions to overspin a black hole? Recall that overspinning a black hole (which means increasing the angular momentum beyond the extremal limit) is one way that people have historically tried to violate cosmic censorship in asymptotically flat space-times [57]. In that context, it has been found that as black holes approach the extremal limit, they repel particles with the same angular momentum more and more strongly, and so it seems to be impossible to overspin a black hole by throwing more matter in. However, in asymptotically AdS spaces, the boundary conditions give us a new tool that we can exploit to try to dynamically increase the angular momentum beyond the extremal limit.

Consider the so-called "boosted black brane" solution in 4 dimensions, which is an asymptotically AdS planar black hole with momentum along one of the boundary directions (we will periodically identify the boundary coordinate y which is why we refer to this momentum as *angular* momentum):

$$ds^2 = \frac{L^2}{z^2}\left(-\frac{f}{K}dt^2 + f^{-1}dz^2 + K(dy - \omega dt)^2 + dx^2\right) \tag{5.1}$$

where

$$f = 1 - L^{-3} M z^3 \tag{5.2}$$

$$K = 1 + \frac{\beta^2}{1-\beta^2} L^{-3} M z^3 \tag{5.3}$$

$$\omega = \beta^{-1}(1 - K^{-1}). \tag{5.4}$$

The temperature is given by

$$T = \frac{3M^{1/3}}{4\pi L^{4/3}} \sqrt{1-\beta^2}. \tag{5.5}$$

The question is: can we destroy a black hole like this by using the boundary conditions to dynamically force β to exceed 1? The boundary metric for this solution is the same for all values of β (it is just the flat metric) so the answer at first sight appears to be no. However, suppose we introduce some x dependence, but make the gradients small enough that the solution still looks like the boosted black brane locally. In that case, the answer is yes.

First, note that as $\partial/\partial y$ is Killing we can shift ω by a constant by redefining y. It is therefore only the difference between ω on the boundary and ω on the horizon that is physically significant. We denote this difference $\Delta\omega$. For a boosted black brane, $\Delta\omega = \beta$. Now for a stationary solution with a Killing horizon, ω on the horizon should be constant. Therefore, if we use the boundary conditions to specify a profile $\omega(x)|_{z=0}$ on the boundary such that $\max \omega(x) - \min \omega(x)|_{z=0} > 2$, there will be some value of x for which $\Delta\omega(x) > 1$. We expect the solution to look locally like a boosted black brane, but if that is the case at this value of x, we would need to have $\beta > 1$. Imposing such boundary conditions therefore looks like a promising way to destroy a black hole.

We can also try to understand this from the field theory perspective on the boundary using AdS/CFT. The CFT should be strongly interacting, but as a toy example, suppose we have a free massless scalar field on the following background

$$ds^2 = -dt^2 + dx^2 + (dy + a(x,y)dt)^2. \tag{5.6}$$

Suppose that the function $a(x,y)$ varies sufficiently slowly that we can use the hydrodynamic approximation: we can calculate thermodynamic quantities at (x_0, y_0) by taking $a(x,y) = a(x_0,y_0)$ to be constant in a local region. This matches the approximation we made above when we assumed that the bulk metric functions had small gradients in x. Solutions to the scalar field equation of motion in this region can then be decomposed into non-interacting modes $e^{-i(\omega + k_y a)t + ik_y y + ik_x x}$ where $\omega^2 = k_x^2 + k_y^2$. The partition function of a single mode, after

quantization, is given by:

$$Z = \sum_n e^{-\beta n(\omega + k_y a)}. \tag{5.7}$$

For modes with momentum directed in the y direction, we have $k_y = \pm|\omega|$. As $a \to \pm 1$, the ratio of this geometric series can then approach 1 for such modes, and their occupation number diverges. Macroscopically, this causes the total momentum in the y direction to diverge. When $|a| \geq 1$, a thermal equilibrium state no longer exists. Geometrically, points with $|a(x,y)| \geq 1$ form the ergoregion. Naively, we might then expect problems to arise as soon as an ergoregion forms in the boundary metric.

A subtlety arises when the source function a is independent of y, as it was in the gravitational solutions we discussed. In this case we can shift a by a constant using a coordinate transformation $y' = y + ct$ which sends a to $a - c$. This means the inequality $|a| \geq 1$ is no longer gauge invariant and the above discussion cannot apply. The reason it breaks down is that there is now an additional conserved quantity to consider when we construct the partition function: the momentum in the y direction. This must be included along with an associated chemical potential. The new partition function is:

$$Z = \sum_n e^{-\beta n(\omega + k_y a) + \beta \mu n k_y} \tag{5.8}$$

and the new requirement for the sum to converge is that

$$a - 1 < \mu < a + 1. \tag{5.9}$$

For an equilibrium solution, μ must be independent of x, and so this inequality implies a necessary condition on the source function $a(x)$: its maximum and minimum cannot differ by more than 2. This is exactly what we found on the gravitational side. Equivalently, there must exist *some* coordinates in which the boundary metric does not contain an ergoregion.

With this we are now ready to propose a plan for how to form naked singularities in vacuum asymptotically AdS spaces. We begin with pure AdS, and then deform the boundary metric according to Equation 5.6, with time dependence introduced into a. We dynamically increase a until it exceeds 1 (in the case that a has y dependence) or until its range exceeds 2 (in the case that it is independent of y). At this point, at least working within the small gradient approximation, we should expect something dramatic to happen. There should be no non-singular stationary solution that the system could settle down to.

There are two potential problems with this, arising from the fact that an ergoregion in the boundary metric appears to be essential in order to get singular behaviour. The first is that a superradiant instability might set in near the boundary when the y symmetry is broken. The

fact that the ergoregion is on the boundary means it is not completely clear if a superradiant instability will exist or not, since ingoing waves are partially absorbed by the horizon and return with smaller amplitude. This can compensate for the enhanced scattering off the ergoregion. However, in [26] it is shown that in global AdS, with a compact Killing horizon, if the horizon Killing field becomes space-like anywhere outside the horizon then the solution will be unstable. Given this result, it is likely that our solutions will be unstable as well. If we assume a y symmetry in our numerics, we might therefore get misleading, non-generic, results. The second problem is that there may be no positivity of energy theorem when the boundary metric contains an ergoregion. If that is the case, although we might observe singular behaviour, this would not be particularly interesting. We already have examples where we can use unphysical negative energy matter to form naked singularities, and our examples might belong in the same category as these. We will discuss both of these problems after presenting our results. From now on in this Chapter we work in units where $L = 1$.

5.2 Stationary Solutions

Before studying the full time dependent case, we can study stationary profiles $a(x)$. If the rough hand-wavy discussion above is correct, we should expect that when the size of the profile becomes sufficiently large, non-singular stationary solutions will no longer exist. In the high temperature limit (when the gradients in x in units of temperature are small) we might expect this to happen precisely when the range of values of a exceeds 2. Furthermore, studying the behaviour of the stationary solutions as the amplitude of the boundary profile approaches its maximum could tell us how the time-dependent solutions will behave when the profile varies very slowly in time.

5.2.1 Compact Case

We now change notation to better match that found in [14]. Consider a boundary metric of the following form

$$ds_\partial^2 = -dt^2 + dX^2 + (dW - \omega(X)dt)^2 \tag{5.10}$$

where X and W are both periodic with periods $2\pi/k_X$ and $2\pi/k_W$ respectively. The source function is now denoted $\omega(X)$, and we choose to impose a profile

$$\omega(X) = a\cos k_X X. \tag{5.11}$$

Note that if $a > 1$, there is a boundary ergoregion (and the range of values of ω exceeds 2), whereas if $a < 1$ there is none, so we write $a_{\text{ergo}} = 1$. We construct stationary solutions numerically using the DeTurck method [33], for various values of a and temperatures T. Note that stationary solutions should also be characterised by their total angular momentum, J. In the numerics, this is imposed by the boundary condition we use for ω on the horizon. But in the time dependent case, the angular momentum will be conserved, and so is not up to us to specify. In particular, we want to imagine starting from pure AdS, where the total angular momentum is zero. We are therefore interested in the stationary solutions with zero total angular momentum. These will be the stationary solutions for which ω vanishes on the horizon. The symmetry of our profile then ensures that the total angular momentum of our stationary solutions is always zero.

For all temperatures, we do find a maximum value a_{max} above which no stationary solutions appear to exist. Furthermore, as a approaches a_{max}, the space-time curvature diverges. To see this, we can monitor the square of the Weyl tensor $C_{abcd}C^{abcd}$ throughout the spacetime, and find its maximum value

$$C_{\text{max}} \equiv \max_{\mathscr{M}} |C_{abcd}C^{abcd}|. \tag{5.12}$$

We plot this quantity as a function of a in Figure 5.1 for $T/k_X = 0.239$ (top curve) and $T/k_X = 0.0119$ (bottom curve). This is suggestive that in the time-dependent case, a naked singularity might indeed form. In Figure 5.2 we plot a_{max} as a function of the temperature. We find that when the temperature is large, $a_{\text{max}} = a_{\text{ergo}}$ to within numerical error, agreeing with the intuition of the previous section. When the temperature is small, $a_{\text{max}} > a_{\text{ergo}}$, so it is always necessary to have an ergoregion on the boundary in order to observe this singular behaviour.

Finally, we can ask whether the situation changes if we break the symmetry in the W direction. Suppose we take a boundary metric of the following form

$$ds^2_\partial = -dt^2 + (dX - \omega(W)dt)^2 + (dW - \omega(X)dt)^2. \tag{5.13}$$

The calculations are much more time consuming since we are now solving ten coupled three-dimensional nonlinear partial differential equations. Nevertheless, we reach similar conclusions. Again we find that solutions exist up to a maximum value a_{max} and that this can be larger than $a_{\text{ergo}} = 1/\sqrt{2}$.

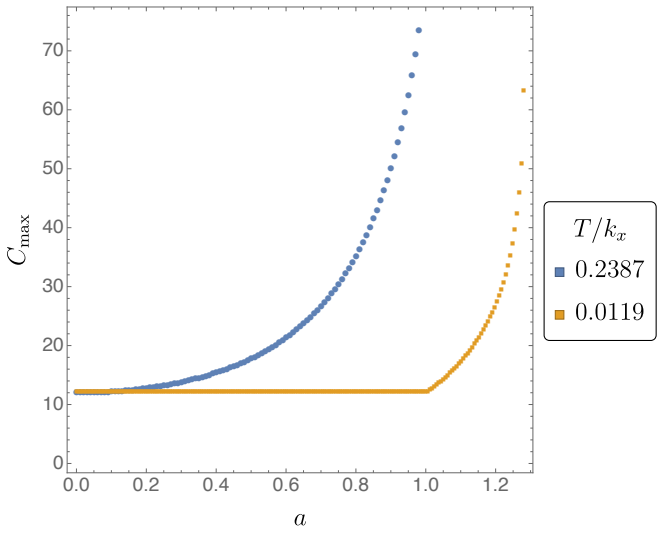

Fig. 5.1 $C_{\max}$ as a function of a, depicted for $T/k_X = 0.2387$ (top curve) and $T/k_X = 0.0119$ (bottom curve). The kink in the bottom curve corresponds to the interchange of two local maxima.

5.2.2 Non-Compact Case

We can also try to observe similar behaviour with a planar boundary metric. Suppose we take a boundary metric of the following form

$$ds_\partial^2 = -dt^2 + dr^2 + r^2\left(d\phi - \omega(r)dt\right)^2 \tag{5.14}$$

with

$$\omega(r) = ap(r) \tag{5.15}$$

such that $rp(r) \to 0$ as $r \to \infty$. If ω varies slowly with r (or if the temperature is large) the same arguments that we had before would suggest that once the difference between the horizon value of $r\omega$ and the boundary value of $r\omega$ exceeds 1, problems should occur. But now, if we want a finite value of the total angular momentum, the horizon value of ω must vanish, so that the difference between boundary and horizon values is 0 for large r. This means that even though we have a symmetry in ϕ, problems should occur as soon as $r\omega(r)$ exceeds 1 anywhere. It is not necessary that its range exceeds 2. Again, this is equivalent to there being an ergoregion in the boundary metric. We can also understand this from the fact that angular momentum is no longer conserved in the time-dependent solutions, in the sense that the final stationary state which we approach asymptotically need not have the same angular momentum that is present initially. Angular momentum can now be radiated towards infinity.

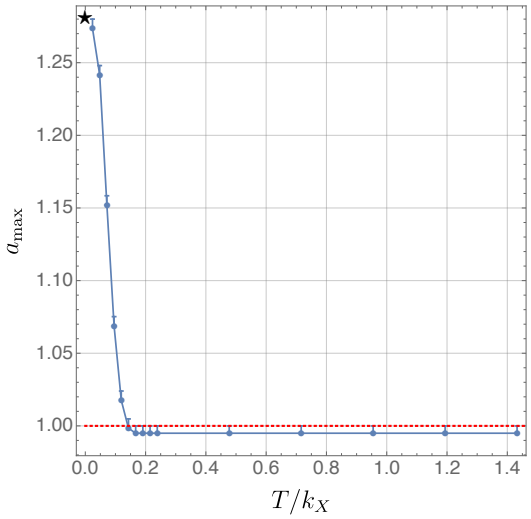

Fig. 5.2 $a_{\max}$ as a function of T/k_X. The black star is the $T = 0$ result and the dotted red line is $a = a_{\text{ergo}} = 1$.

We again construct stationary solutions numerically using the DeTurck method, for various values of a, T, and profiles $p(r)$. Typically, we choose profiles of the form

$$\omega(r) = \frac{a}{(1 + r^2/\sigma^2)^{n/2}}. \tag{5.16}$$

Since the boundary metric is now only determined up to conformal rescalings, we choose to fix $\sigma = 1$ in the numerics. For all temperatures and profiles, we again find a maximum value $a_{\max}$ above which no stationary solutions seem to exist. Furthermore, as a approaches $a_{\max}$, the spacetime curvature again diverges. We plot $C_{\max}$ as a function of a in Figure 5.3 for $n = 8$ at $T = 0$ (left) and $n = 4$ at $T = 0.9/4\pi$ (right). In Figure 5.4 we plot $a_{\max}$ as a function of the temperature when $n = 4$. Again, when the temperature is large, $a_{\max} = a_{\text{ergo}}$ to within numerical error. When the temperature is small, $a_{\max} > a_{\text{ergo}}$, so it is again necessary for an ergoregion to be present on the boundary in order to see singular behaviour.

5.3 Time Dependent Solutions: The Compact Case

We have also studied the time dependent solutions in the compact case using the numerical method presented in Chapter 3. The goal is to see if large curvatures become visible to distant observers when the amplitude is made large. We chose $k_X = k_W = 1$ and have collected

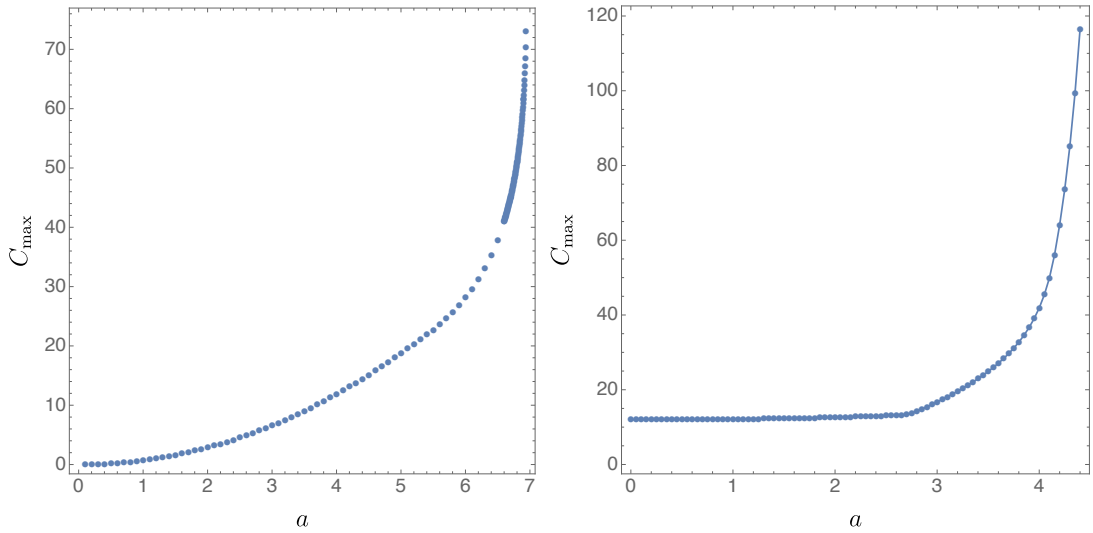

Fig. 5.3 $C_{\max}$ as a function of a, computed for $n = 8, T = 0$ (left) and $n = 4, T = 0.9/4\pi$ (right).

results for a cosine boundary profile at various final amplitudes:

$$\begin{aligned} \omega(t,X) &= (1-\operatorname{sech} 5t)\omega_f(X) \\ \omega_f(X) &= a_0 \cos(X) \\ a_0 &= 0.7, 0.9, 1.0, 1.1, 1.3. \end{aligned}$$

This choice of time dependence causes the amplitude of the profile to increase smoothly from an initial value of 0 to a maximum value a_0, with $\omega(1,0) > 0.98a_0$ and $\omega(2,0) > 0.9999a_0$.

We find that when $a_0 < 1$, the solution settles down to a stationary solution at late times as expected. These solutions are presented in Section 5.3.1. But when $a_0 > 1$ so that an ergoregion is present on the boundary, the solutions do not settle down. Instead, a component of the boundary energy-momentum tensor, representing the momentum density in the W direction, grows linearly with time. We denote this component

$$j = \langle T^t{}_W \rangle. \tag{5.17}$$

Since both $\partial/\partial t$ and $\partial/\partial W$ are Killing vector fields of the late time boundary metric, j is physically significant and the growth is not merely an artefact of the choice of coordinates. For the intermediate $a_0 = 1$ case, the solution also showed no signs of settling down, but in this case the growth in the momentum density was not linear. We present these solutions in Section 5.3.2.

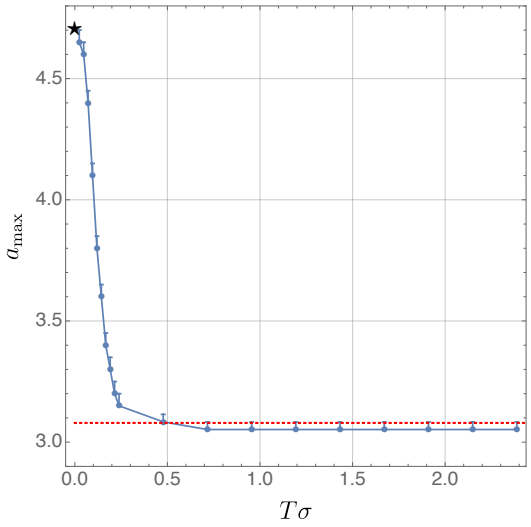

Fig. 5.4 $a_{\max}$ as a function of T, computed for $n = 4$. The black star is the $T = 0$ result and the dotted red line is a_{ergo}.

We can understand this behaviour as follows. Our initial temperature is $\frac{3}{4\pi}$. From the stationary solutions of the previous section, we can see that this temperature is large enough that the maximum amplitude is indistinguishable from $a_{\text{ergo}} = 1$ to within numerical error. We should therefore expect no stationary solutions to exist at this temperature almost as soon as an ergoregion forms in the boundary metric. This explains why our solutions with $a_0 \geq 1$ did not settle down during the time that we can evolve them for. There is an additional complication to consider, because the temperature of our solutions changes with time. In the solutions which eventually settle down, we observe that it always decreases (we give an explanation for why it *decreases* in Section 5.3.1). As the temperature decreases, $a_{\max}$ increases, and so we have to consider whether a temperature could be reached with $a_{\max} > a_0$. We discuss this issue in Section 5.3.2.

In order to demonstrate the dependence of $a_{\max}$ on temperature explicitly with the time-dependent numerical scheme, we have also generated solutions where the initial temperature is halved, so $T = \frac{3}{8\pi}$. This is equivalent to making $\omega_f(x)$ oscillate twice as fast, and this is how we actually modify the numerics in practice. In this case we are able to find solutions with $a_0 \geq 1$ which do settle down. These solutions are presented in Section 5.3.3.

Finally, one might be worried that because we assume a symmetry in the W direction, the behaviour that we observe may not be generic. In order to check this, we have also constructed some numerical solutions to the full $3+1$ problem in which no such symmetry assumption is made. We are not able to evolve these solutions very far, but they appear to be behaving similarly. We present these results in Section 5.3.4.

5.3.1 $a_0 < 1$ Solutions

In Figure 5.5, for the $a_0 = 0.7, 0.9$ solutions we plot the maximum value of the momentum density on the boundary, and its time derivative, as a function of time. In both cases the solution appears to stabilize at late times. It is interesting to consider the parameters characterizing the final stationary solution. The total momentum (obtained by integrating the momentum density over the boundary) must be conserved, and so vanishes both on the initial time slice and on the final stationary solution. However, the energy and the temperature both change. Interestingly, the final temperature is *lower* than the initial temperature. Our initial conditions have temperature $\frac{3}{4\pi} \approx 0.24$ but for the $a_0 = 0.7$ and $a_0 = 0.9$ solutions we find final temperatures of 0.21 and 0.18 respectively. Using this measured value of the temperature, we are able to directly compare the endpoint of our evolution with the stationary solutions of the previous section, and we find good agreement. This is a reassuring check on the accuracy of the numerics.

We can understand the decrease in the temperature as follows. Suppose that we were to increase the profile more slowly, so that the adiabatic approximation is valid and the time-dependent solution approximately moves through the space of stationary solutions of increasing amplitude. The entropy of the stationary solutions at fixed temperature diverges as the amplitude approaches 1, but if our time-dependent solution changes adiabatically then its entropy is conserved. The temperature must therefore decrease in order to satisfy this condition. In fact, by choosing an amplitude sufficiently close to the maximum one, and by varying the profile sufficiently slowly, we should in principle be able to make the temperature of our final stationary black hole arbitrarily small.

5.3.2 $a_0 \geq 1$ Solutions

In Figure 5.6, we plot the maximum value of the momentum density for the solutions corresponding to $a_0 = 1$, $a_0 = 1.1$ and $a_0 = 1.3$. We stop each evolution when our estimate of the error, as measured by the expansion of null geodesics at $z = 1$, becomes larger than 10^{-3}.

For these profiles, the momentum density grows in time long after the boundary profile has settled down. For the $a_0 = 1.1$ and $a_0 = 1.3$ solutions, this growth appears approximately linear, and the gradient is larger for larger amplitudes. For the $a_0 = 1.3$ solution, the amplitude is larger than $a_{\max}$ for any value of the temperature, and so we expect the growth in the momentum density in this case to continue indefinitely. For the $a_0 = 1$ and $a_0 = 1.1$ solutions on the other hand, it is not immediately clear what will happen in the distant future. These amplitudes are above the maximum amplitude corresponding to the initial temperature ($\frac{3}{4\pi}$),

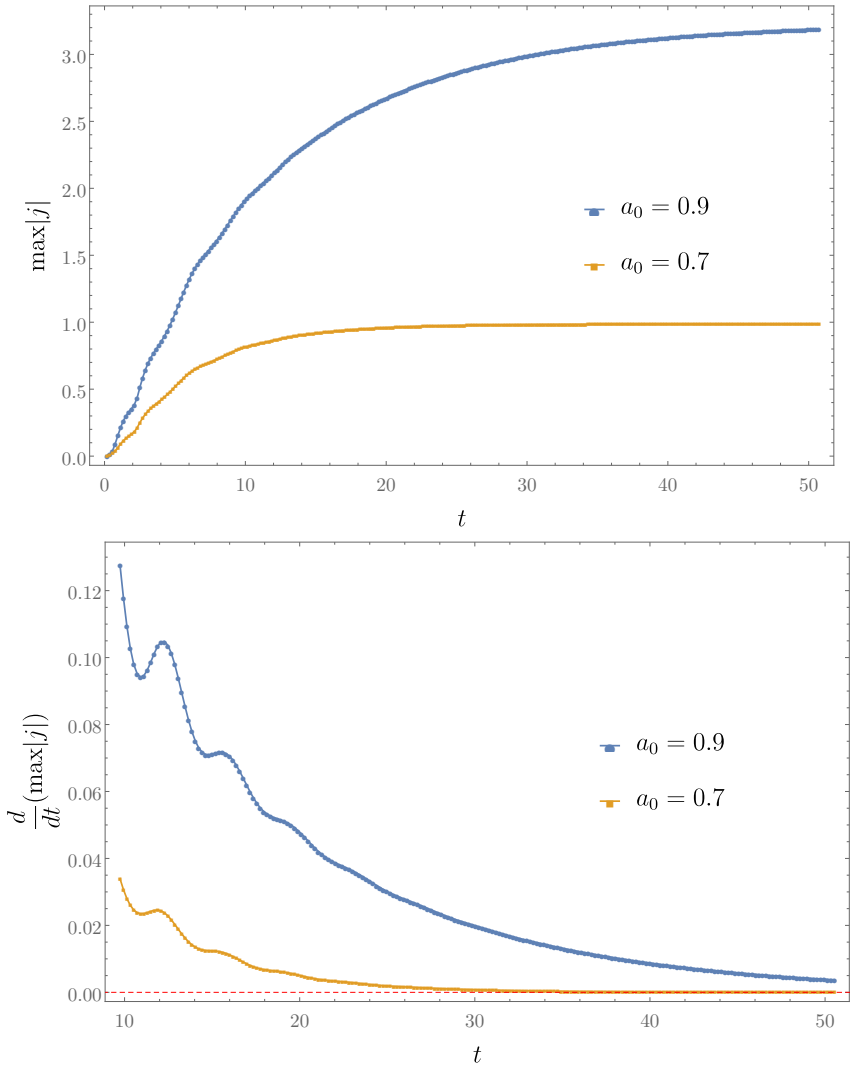

Fig. 5.5 The maximum of the boundary momentum density, and its time derivative, as a function of time for the $a_0 = 0.7$ and $a_0 = 0.9$ solutions.

but they are less than the zero temperature maximum, and the temperature in our time dependent solutions is not fixed. However, we have an argument for why these solutions should not be able to settle down either. The energy is conserved after about 1 unit of time once the boundary metric becomes stationary, which means that if the system were to settle down, we know which stationary solution it would have to settle down to. We also know the entropy of this stationary solution. But the entropy of our dynamical solutions is diverging rapidly along with the momentum density (assuming this is given accurately by the area of the apparent horizon). Since the entropy cannot decrease, once it has exceeded the value of the corresponding stationary solution, it should be impossible for the system to settle down.

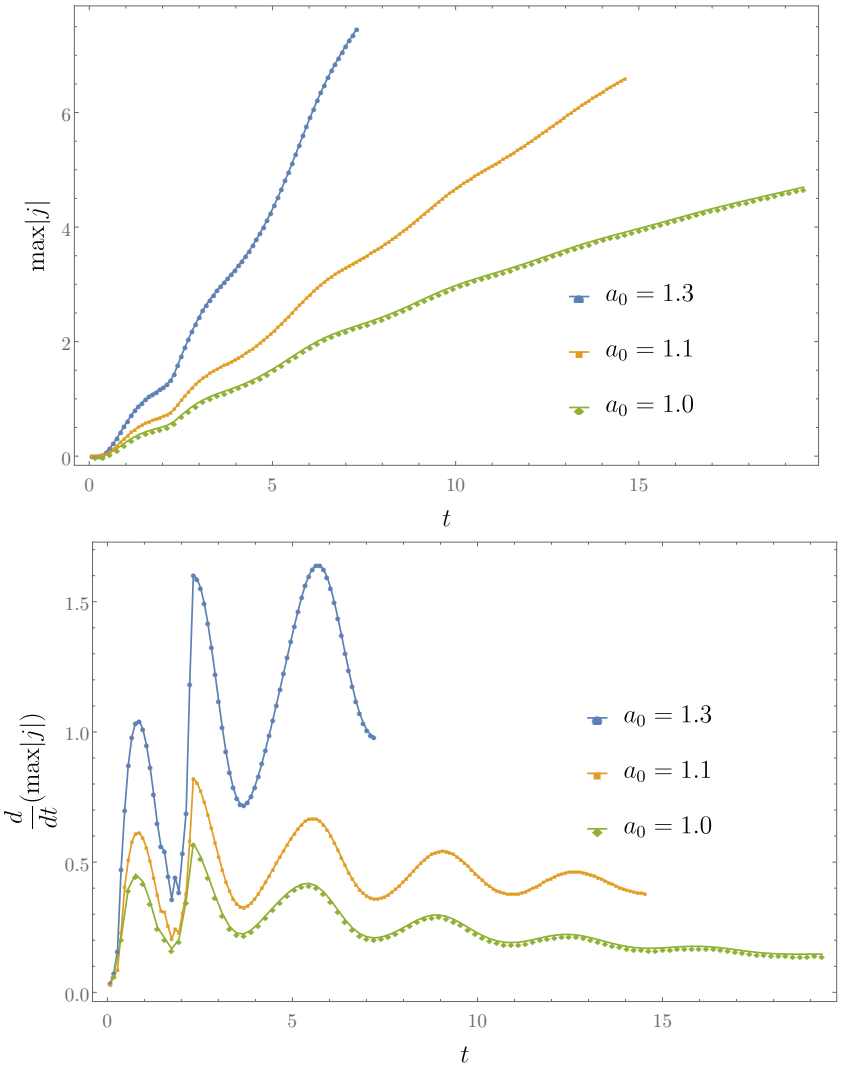

Fig. 5.6 The maximum of the boundary momentum density, and its time derivative, as a function of time for the $a_0 = 1.0$, $a_0 = 1.1$, and $a_0 = 1.3$ solutions.

5.3.3 $T = \frac{3}{8\pi}$ Solution

In Figure 5.7, we plot the maximum value of the momentum density for $a_0 = 1.0$ when the initial temperature is halved. The numerical error in this case grows more rapidly, and we cannot evolve beyond $t = 3$ without the expansion of null geodesics on $z = 1$ becoming large. However, we do see the first indications that the solution is settling down. This supports the observation made in the previous section that the maximum amplitude increases with decreasing temperature.

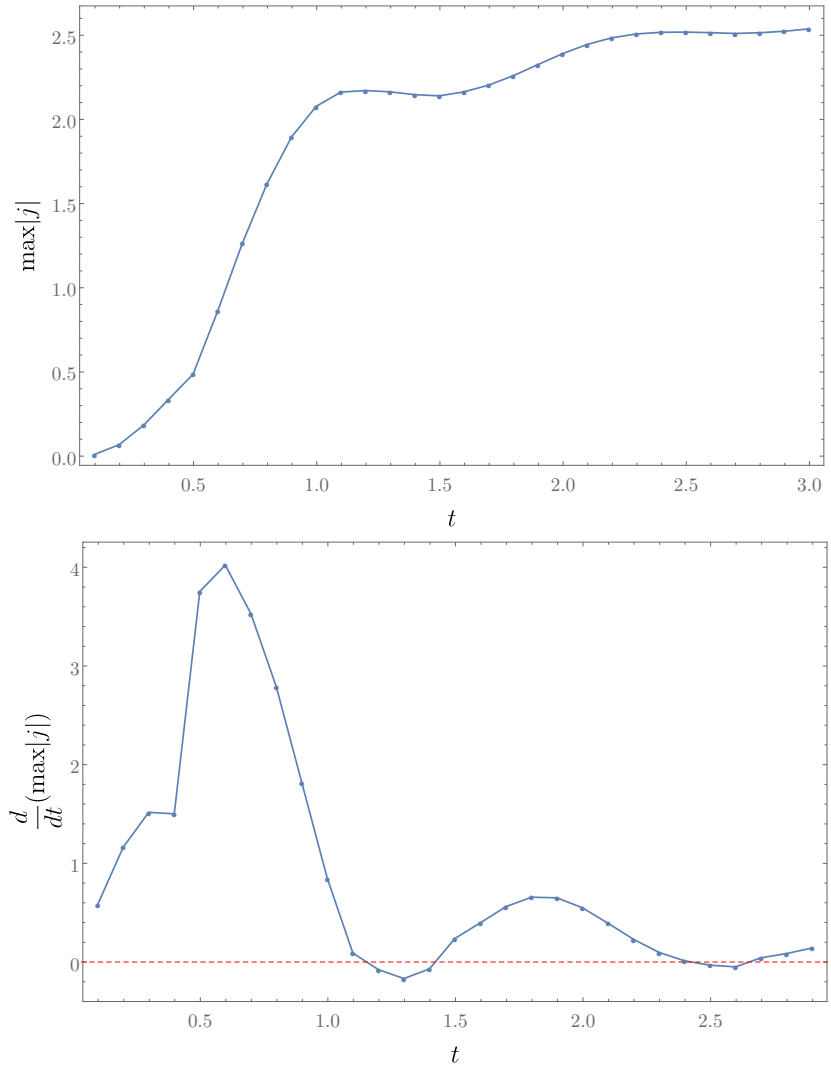

Fig. 5.7 The maximum of the boundary momentum density, and its time derivative, as a function of time for the $a_0 = 1.0$ solution with initial temperature $T = \frac{3}{8\pi}$.

5.3.4 $3+1$ Solutions

The solutions presented so far assumed a symmetry in the W direction, and so it is not completely clear whether the behaviour we observe is generic or not. To test this, we have attempted to simulate the full $3+1$ problem with no symmetry. These solutions appear to be behaving in a similar way, although unfortunately we have not been able to evolve them very far before they become numerically unstable. We break the symmetry by imposing the following boundary metric

$$ds_\partial^2 = -dt^2 + (dX - \omega(W)dt)^2 + (dW - \omega(X)dt)^2 \tag{5.18}$$

where the function ω is chosen in the same way as before. The results for $a_0 = 1.3$ are presented in Figure 5.8. We are only able to evolve to about 1 unit of time before the numerical error grows unacceptably large, but already the momentum density is diverging rapidly.

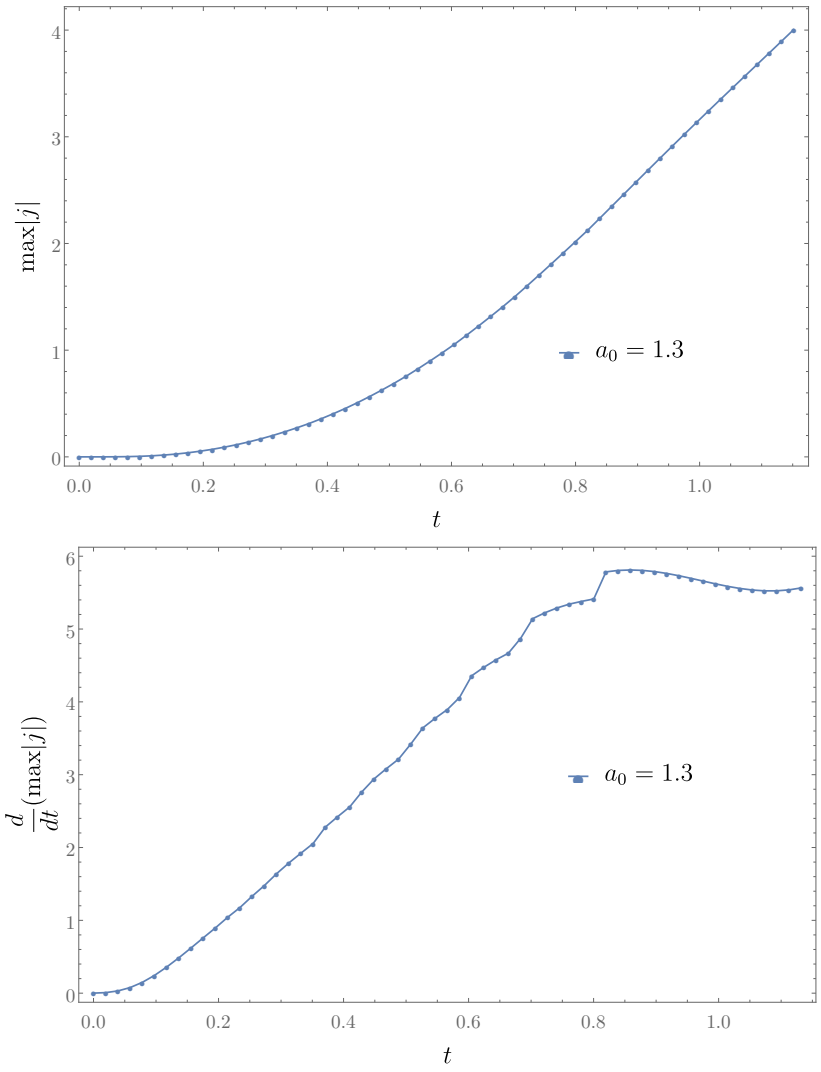

Fig. 5.8 The maximum of the boundary momentum density, and its time derivative, as a function of time for the $3+1$ dimensional $a_0 = 1.3$ solution.

5.4 Is Cosmic Censorship Really Violated?

5.4.1 The Space Time Curvature

We have presented examples in which an observer at the boundary is able to see gauge-invariant quantities rapidly diverging. We want to say that this is a violation of Cosmic Censorship in the sense discussed in Chapter 2. However, we have not yet said whether the space time curvature itself is blowing up. Do we have a naked singularity or not? In the stationary solutions, we saw that the Weyl tensor diverges as you approach the maximum amplitude, suggesting that a naked singularity would form. But for the time dependent solutions we have obtained, in the compact case at finite temperature, it looks like the space time curvature is in fact *not* diverging. We plot the maximum value of the Kretschmann scalar for the $a_0 = 1.3$ solution in Figure 5.9.

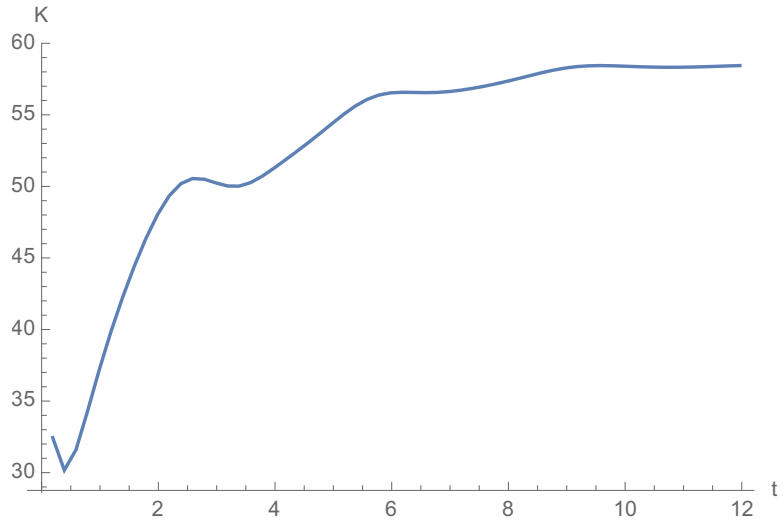

Fig. 5.9 The maximum value of the Kretchmann scalar in the $a_0 = 1.3$ solution as a function of time.

How can this be? Firstly, we do not vary the boundary profile slowly (to ensure that we can obtain results in a reasonable time), so the argument that the time dependent solution should behave like a family of stationary solutions fails for that reason. But also, even if we were to vary the profile slowly, the temperature would not be constant, which is another reason why our solution cannot behave exactly like a family of stationary solutions at fixed temperature. It is possible that if we were to obtain time dependent solutions in the planar case, then they *would* behave more like the corresponding family of stationary solutions, and the space time curvature would diverge. In that case the temperature would be fixed. We have attempted to simulate this at zero temperature using the numerical method of Chapter 4,

but we have not been able to evolve these solutions for long enough to confirm or reject this possibility. Whether or not naked curvature singularities can really form in our examples is still an open question.

5.4.2 Superradiant Instability

Because our potential counter-examples to Cosmic Censorship all contain an ergoregion, another complication to consider is that a superradiant instability might set in when the symmetry in the W direction is broken. This means that although we were able to find some stationary solutions with amplitude in the range $a_{\text{ergo}} < a < a_{\text{max}}$, there is reason to think that they might be unstable. In fact, we have explicitly checked that they *are* unstable. Solutions in this range should then also, generically, not be able to settle down, even though the amplitude is below a_{max}. It has been proposed that such superradiant instabilities in AdS space times might also violate Cosmic Censorship. However, these violations would be very different from the ones proposed in this thesis. In particular, the violations we propose exhibit large curvatures in large regions of spacetime, whereas naked singularities arising from superradiance would likely involve arbitrarily large curvatures in an arbitrarily small region of spacetime. One thing we need to worry about then is whether this instability will affect the behaviour of our solutions when the symmetry is broken, which could mean that the $2+1$ numerical results are not generic. However, the growth rate of the superradiant instability is likely to be very slow compared to the blow up in the momentum density, and so we expect the latter instability to dominate. We saw that our $3+1$ solutions still began to exhibit momentum blow up, even though we were not able to evolve them for very long.

5.4.3 Positivity of Energy

The most serious problem with our proposed counter-examples is that positivity of energy probably fails as soon as an ergoregion appears in the boundary metric. If this is the case, then our violations of the WCCC would be trivial. It is already known to be possible to form naked singularities if you have access to negative energy matter. One argument for why positivity of energy fails uses AdS/CFT. It seems clear that positivity of energy will fail on the CFT side. Consider the planar case with $a_{\text{ergo}} < a < a_{\text{max}}$. The boundary metric is an asymptotically flat spacetime with an ergoregion and no horizon. Consider first classical or free quantum fields. Classical fields on such spacetimes are known [21] to be unstable since one can construct negative energy solutions by exciting fields in the ergoregion. Since stationary solutions must have zero energy and the energy radiated to infinity is always positive, if the energy is negative initially, it will continue to decrease. Free quantum fields

on such a spacetime exhibit a similar instability: it has been shown [2, 40] that there is no Fock vacuum that is time translation invariant. In other words, there is particle creation in all states. It is also clear that there is no lower bound on the energy for free quantum fields in such a spacetime. This is because excitations localized in the ergoregion can have negative energy, and one can give them arbitrarily large occupation number.

Even at strong coupling, a CFT on a spacetime with ergoregion and no horizon cannot have a minimum energy state[1]. Start with the ground state in Minkowski space and act with a unitary operator in a finite region A. This creates a state with $E > 0$ that looks like the vacuum outside A. By scale invariance, we can make A as small as we want. Now consider our boundary metric and pick a small locally flat region inside the ergoregion. As long as A is small enough, we can insert the above state into this geometry. We can then boost it to give it arbitrarily negative energy.

However, just because positivity of energy fails on the CFT side does not immediately imply that it must fail on the gravity side. Note that even in vacuum asymptotically flat space times, there exist gravitational states with negative energy. The negative mass Schwarzschild solution is one example. The positive energy theorem of GR does not say that no asymptotically flat negative energy states exist, it says that no *non-singular* negative energy states exist. This *might* still be true for our solutions as well. One could imagine that every negative energy state on the CFT would be dual to a gravitational state containing a naked singularity. Indeed, we have tried and failed to construct negative energy non-singular initial data in this set-up, which is weak evidence that positivity of energy might hold after all.

One can also present a purely gravitational argument for why positivity of energy should fail with a boundary ergoregion, though it is slightly weaker than the arguments given above. One can clearly place test particles in the ergoregion and boost them so that their energy is arbitrarily negative. We now want to replace the test particle by a small black hole. There are gluing theorems which ensure that one can add a small black hole in the ergoregion to initial data on a constant t surface [39]. An $O(1)$ boost of this black hole will cause it to contribute negatively to the total energy, and should not result in any singularities in the initial data. Moving the black hole further into the asymptotic region should increase its negative contribution to the energy without bound. However, it is not clear how the backreaction of the black hole on the space time will affect this argument.

What are the implications of this discussion for our results? There are two possibilities we need to consider: positivity of energy holds, or it does not. If it does not, as seems likely, then our naked singularities (if we can actually form naked singularities) are trivial, and we have failed to violate cosmic censorship. In this case, the fact that we always find

[1] We thank D. Marolf for suggesting this argument.

$a_{\max} > a_{\text{ergo}}$ can be taken as evidence in favour of the WCCC in vacuum $3+1$ dimensional asymptotically AdS space times. On the other hand, if positivity of energy does hold, then we may have found a way to violate the WCCC in vacuum $3+1$ dimensional asymptotically AdS space times in a non-trivial way (assuming there are circumstances in which the space time curvature actually does diverge). However, these counter-examples would only work when the dual CFT has energy unbounded from below. In other words, although our counter-examples make sense from the point of view of classical GR, it looks like they cannot be realised as the low energy description of a well behaved quantum gravity theory in the UV. When we look at examples involving an electromagnetic field (where positivity of energy certainly holds) we find the same thing. We can violate the WCCC, but only when there is no good quantum gravity theory in the UV. We discuss this intriguing observation further in Chapter 7. First though, we present the electromagnetic examples.

Chapter 6

Forming Naked Singularities with an Electromagnetic Field

6.1 Motivation

In the previous Chapter, we presented potential violations of the WCCC in asymptotically AdS vacuum space times. However, these examples ended up being somewhat underwhelming. We were not certain that naked curvature singularities would actually form, and even if they did, it was not clear whether these singularities would qualify as violations of the WCCC anyway. In particular, it seemed unlikely that there existed a positivity of energy theorem for our examples. In this Chapter, we present potential violations of the WCCC in asymptotically AdS space times containing an electromagnetic field. We work with the Einstein-Maxwell action

$$S = \frac{1}{16\pi}\int d^4x\sqrt{-g}\left(R + \frac{6}{L^2} - F_{ab}F^{ab}\right). \tag{6.1}$$

This time, we have strong evidence that naked singularities really can form, and they do appear to be genuine violations of the WCCC (in the sense discussed in Chapter 2). There is a positivity of energy theorem for these space times.

In the previous Chapter, we were able to motivate our examples by considering the problem of trying to overspin a black hole, but that argument will not work for charged black holes. This is because the chemical potential of an AdS-Reissner-Nordstrom black hole can be made arbitrarily large without the black hole becoming extremal. Nevertheless, there is still numerical evidence that under the right circumstances, naked singularities might be formed by imposing sufficiently violent boundary conditions on the electromagnetic field. This was first uncovered in [35]. Their original aim was to use the AdS/CFT correspondence

to study localized defects in condensed matter systems. Working in coordinates where the boundary metric takes the form

$$ds_\partial^2 = -dt^2 + dR^2 + R^2 d\phi^2 \tag{6.2}$$

they imposed a boundary electric field

$$f = \frac{aR\gamma}{\sigma^2\left(1+\frac{R^2}{\sigma^2}\right)^{\frac{\gamma}{2}+1}} dt \wedge dR \tag{6.3}$$

and constructed stationary solutions at zero temperature for various values of $\gamma \geq 1$. Due to conformal invariance of the UV theory, only the product $a\sigma$ is physically meaningful, and from now on we will set $\sigma = 1$. Just like the examples of the previous Chapter, they found that there was a critical amplitude $a_{\max}$ above which no stationary solutions could be constructed, at least with a connected horizon. That is to say, there *were* stationary solutions with $a > a_{\max}$, but they necessarily contained so called *hovering black holes*. There was always a charged extremal spherical horizon hovering above the Poincaré horizon, held in stable equilibrium by the balance between gravitational and electrostatic forces. Furthermore, in the stationary solutions without a hovering black hole, the curvature diverged on the horizon as $a \to a_{\max}$. Unlike the vacuum case, it is only at zero temperature that a maximum amplitude is found. At finite temperature, stationary solutions with a connected horizon exist for arbitrarily large amplitude.

We can now explain the proposal for how to violate the WCCC, first outlined in [38], using the same idea that was used in the previous chapter. We impose the boundary condition 6.3 but promote a to be a function of time. We set $a = 0$ initially, starting in vacuum AdS, but then we smoothly increase a to some value beyond $a_{\max}$. It is impossible for a hovering black hole to form dynamically, because we have no charged matter, so if the results of [35] are correct then it should be impossible for these time-dependent solutions to settle down to a smooth stationary solution. Instead, we expect a naked singularity to form. This claim is supported by the fact that the curvature of the stationary solutions diverged on the horizon as $a \to a_{\max}$. We again might expect this to be a good indication as to what will happen in the time dependent solutions if a is varied slowly. It is also supported by studying the behaviour of finite temperature solutions with $a > a_{\max}$ as $T \to 0$ [38]. The curvature diverges on the horizon in that case as well.

6.2 Results

To test this proposal, we have numerically constructed time dependent solutions in the $\gamma = 1$ case using the numerical method from Chapter 4 (with some slight modifications that are outlined in the Appendix). All of our results are presented in units in which $L = 1$. In Chapter 4, we explained how it was useful to construct the coordinates (v, x, ϕ) on the boundary, in which the boundary metric, though still flat, took on the unusual form

$$ds^2|_\partial = -dv^2 + 2\frac{c}{x^2}dvdx + \frac{c^2}{x^2}\left(\frac{dx^2}{1-x^2} + (1-x^2)d\phi^2\right) \tag{6.4}$$

where c is a constant which we set to 1 in our numerics. To get an intuitive understanding of what the coordinate v means, recall that it is related to standard polar coordinates on the boundary (t, R, ϕ) by $v = t - \sqrt{c^2 + R^2}$. At large R, v is effectively an outgoing null coordinate. Working in these coordinates, we choose to make a a function of v in the following way

$$a(v) = a_0\left[1 - \operatorname{sech}(5v)\right]. \tag{6.5}$$

This function increases smoothly from an initial value of 0 to a maximum value a_0, with $a(1) > 0.98a_0$ and $a(2) > 0.9999a_0$. Our choice of a simple v dependence for the boundary electric field comes at the expense of introducing a more complicated t and R dependence. We nevertheless still have the important property that at large t the electric field converges to the stationary profile 6.3 with $a = a_0$. We therefore expect to see a violation of the WCCC based on the arguments in [38].

We can construct the bulk radial coordinate Z as in Chapter 4, but for the presentation of these results we make the further redefinition $\xi = 1 - Z$ so that the boundary lies at $\xi = 1$ and the apparent horizon lies at $\xi = 0$.

For the profile we consider, the critical amplitude was studied in [35] and found to be $a_{\max} \approx 0.678$. We have collected results up to time $v = 7.5$ for five amplitudes: $a_0 \approx 0.4243$, $a_0 \approx 0.5657$, $a_0 \approx 0.7071$, $a_0 \approx 0.8485$, $a_0 \approx 0.9899$. The two solutions with sub-critical amplitude approach a smooth stationary solution at late times as expected. The three solutions with super-critical amplitude have curvature growing without bound on the event horizon at the point $x = 1$. This growth appears to follow a power law in v, and so no singularity forms in finite time. However, by waiting for sufficiently long times we can form arbitrarily large curvatures visible to boundary observers, violating the WCCC.

To demonstrate this, we compute the value of $F^2 = F^{ab}F_{ab}$ on the apparent horizon and look at how it changes with v. This is a gauge invariant scalar, so a divergence in F^2 indicates the formation of a singularity. We can also use the equations of motion to show that it implies

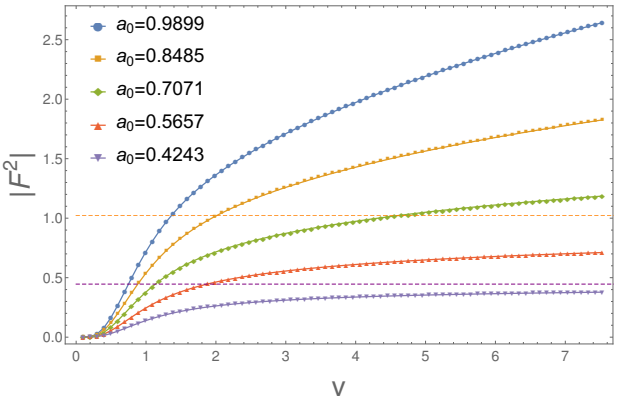

Fig. 6.1 $|F^2|$ at $\xi = 0, x = 1$ as a function of v for five different values of a_0. For the sub-critical amplitudes, the value of $|F^2|$ on the horizon in the corresponding stationary solution can be deduced analytically [35] and is shown as a dotted line.

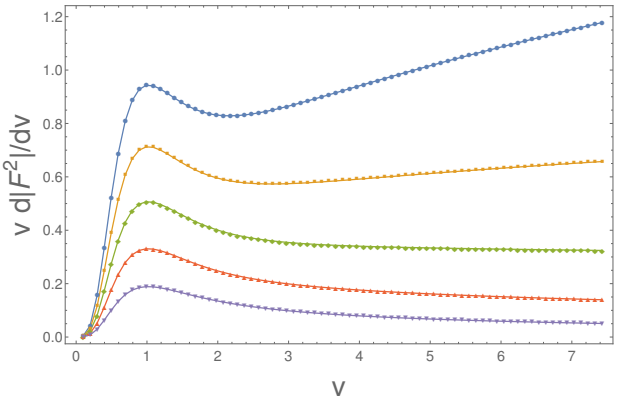

Fig. 6.2 $v\frac{d(F^2)}{dv}$ at $\xi = 0, x = 1$ as a function of v for five different values of a_0. The symbols and colours are the same as in Fig. 6.1.

a divergence in the space-time curvature as well. The Einstein-Maxwell equations imply that

$$R_{ab}R^{ab} = \frac{36}{L^4} + 4\left(F_a{}^c F_{bc} F^{ad} F^b{}_d - \frac{1}{4}(F^2)^2\right) \tag{6.6}$$

and we have checked that in our solutions the second term is proportional to $(F^2)^2$. A divergence in F^2 therefore implies a divergence in the curvature invariant $R_{ab}R^{ab}$.

In Figure 6.1 we plot $|F^2(v)|_{\xi=0,x=1}$ for our five solutions. In all five cases, the magnitude of F^2 is increasing with time, with decreasing derivative. The important question is whether F^2 will converge to some finite value, or whether its magnitude will continue to grow indefinitely. To address this we need to check whether its derivative is tending to zero faster than $1/v$. In Figure 6.2 we plot $v\frac{\mathrm{d}|F^2|}{\mathrm{d}v}|_{\xi=0,x=1}$ for the five solutions. The solutions

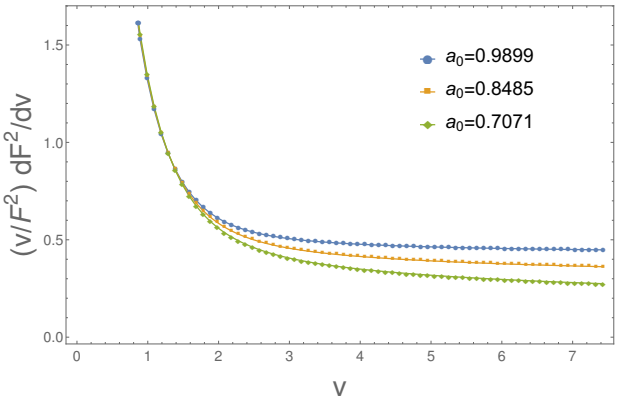

Fig. 6.3 $(v/F^2)\frac{\mathrm{d}(F^2)}{\mathrm{d}v}$ at $\xi = 0, x = 1$ as a function of v for three different values of a_0.

of sub-critical amplitude are consistent with non-divergent growth in F^2, as $v\frac{\mathrm{d}|F^2|}{\mathrm{d}v}|_{\xi=0,x=1}$ appears to decay as v increases. The solutions of super-critical amplitude indicate a divergent growth in F^2. For the solutions with the two largest amplitudes, $v\frac{\mathrm{d}|F^2|}{\mathrm{d}v}|_{\xi=0,x=1}$ has started to grow as v increases. We also expect the $a_0 = 0.7071$ solution to diverge, as it is super-critical, but it is difficult to deduce this with confidence from Figure 6.2. We have continued to evolve this particular amplitude beyond $v = 10$ and find that, although $v\frac{\mathrm{d}|F^2|}{\mathrm{d}v}|_{\xi=0,x=1}$ has still not begun to grow, it does not appear to be decaying towards 0. This could be indicative of logarithmic growth in F^2 or, more likely, power law growth with a very small exponent. This can be understood from the fact that this amplitude is very close to the critical one.

It is interesting to ask how fast F^2 is diverging in the super-critical solutions. If we assume that its late time growth is governed by a power law $F^2 \sim v^\gamma$ then the logarithmic derivative $\frac{v}{F^2}\frac{\mathrm{d}F^2}{\mathrm{d}v}|_{\xi=0,x=1}$ would equal the exponent γ. In Figure 6.3 we plot the logarithmic derivative of our super-critical solutions. The results are consistent with power law growth at late times, with an exponent that increases with the amplitude.

6.3 Are Large Curvatures Visible to Distant Observers?

We have so far presented evidence that the curvature is growing on the *apparent* horizon $\xi = 0$. However, the apparent horizon itself will generically lie inside the event horizon and so will not be visible to distant observers. In numerical investigations of the WCCC, it is usually not possible to locate the event horizon, and instead it is assumed that singular behaviour on the chosen apparent horizon must lead to singular behaviour on the event horizon as well. We can take the same approach here, but it would be preferable to show explicitly that it is possible for a null geodesic to travel from a region of arbitrarily large

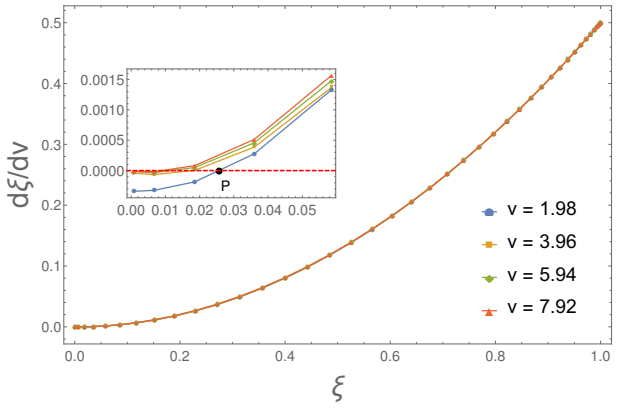

Fig. 6.4 Coordinate velocity of an outgoing null geodesic along $x = 1$ for the $a_0 = 0.7071$ solution at various times. The inset plot depicts small ξ.

curvature out to the conformal boundary. We claim that our results allow us to do this. We have evidence that the apparent horizon is approaching the true event horizon at late times.

In Figure 6.4 we plot the coordinate velocity $\frac{d\xi}{dv}$ of an outgoing null geodesic along $x = 1$ as a function of ξ for the amplitude $a = 0.7071$ solution at times $v \approx 1.98, v \approx 3.96, v \approx 5.94, v \approx 7.92$. We find a function which is increasing and positive almost everywhere except for very close to the apparent horizon, $\xi = 0$. If this plot were independent of time, then an outgoing null geodesic to the right of the zero (marked with the letter P in Fig. 6.4 for the $v = 1.98$ case) would eventually reach the conformal boundary. An outgoing null geodesic to the left of the zero would fall towards $\xi = 0$. The zero itself would mark the position of the event horizon, although the relevant quantities are so small here that we should be worried about numerical error.

We cannot actually identify the event horizon at any particular time because the solution *is* time dependent. However, the plots show that at late times it is only changing very slowly. It appears to be converging to some time independent function, and importantly, the zero is moving leftwards towards the apparent horizon ($\xi = 0$). This suggests that the coordinate velocity at late times is converging to a function of ξ which is positive and increasing for *all* $\xi > 0$, with a zero exactly at the apparent horizon $\xi = 0$. If this were true, then any positive ξ coordinate would eventually be connected to the conformal boundary by an outgoing null geodesic and the apparent horizon would be approaching the event horizon at late times. To check this, in Figure 6.5 we plot the coordinate velocity at $\xi = 0$ itself to show that it is indeed approaching zero with increasing v.

A final possible concern is that even if the apparent horizon approaches the event horizon at late times, and even if the curvature on the apparent horizon is increasing without bound, the approach may be such that the curvature on the event horizon remains bounded. However,

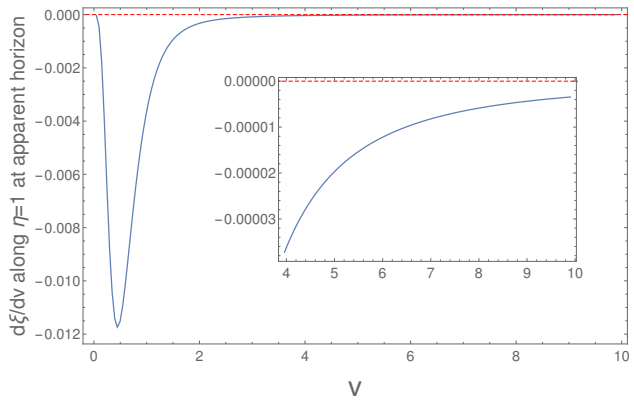

Fig. 6.5 Coordinate velocity of an outgoing null geodesic along $x = 1$ at $\xi = 0$ for the $a_0 = 0.7071$ solution as a function of v. The inset plot depicts late v.

this interpretation does not appear to be consistent with our results. One way to argue that the curvature is diverging on the event horizon is as follows. Given an arbitrarily large bound C :

- after some finite time, by extrapolating our numerical results, we will have $R_{ab}R^{ab} > C$ on the apparent horizon $\xi = 0$.
- By continuity, at the same time there will be a point with small positive ξ coordinate, $\xi = \delta$, where the curvature also violates this bound.
- After some additional finite time, by extrapolating our numerical results again, the point with $\xi = \delta$ will be visible to boundary observers.
- If we additionally assume that the curvature has not decreased at $\xi = \delta$ in this time, then we now have a point with $R_{ab}R^{ab} > C$ visible to boundary observers.

The assumption that $R_{ab}R^{ab}$ is always increasing with v for fixed (ξ, x) was essential to this argument, and this does turn out to be the case, at least over the range of v values for which we have numerical results. To show this, in Figure 6.6, F^2 is plotted along $x = 1$ for the $a_0 = 0.9899$ solution at various times.

6.4 Checks on Numerical Accuracy

Our results provide convincing evidence that the WCCC is violated. Given the significance of this result, it is important to check that the numerical results are accurate. We explained in Chapter 3 that computing the expansion on the apparent horizon is one way of monitoring the numerical error (equivalent to checking that the constraint equations are satisfied away

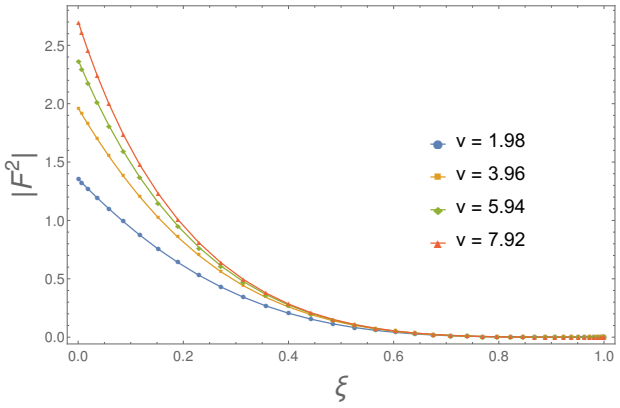

Fig. 6.6 Plot of $|F^2|$ against ξ along $x = 1$ for the $a_0 = 0.9899$ solution at various times.

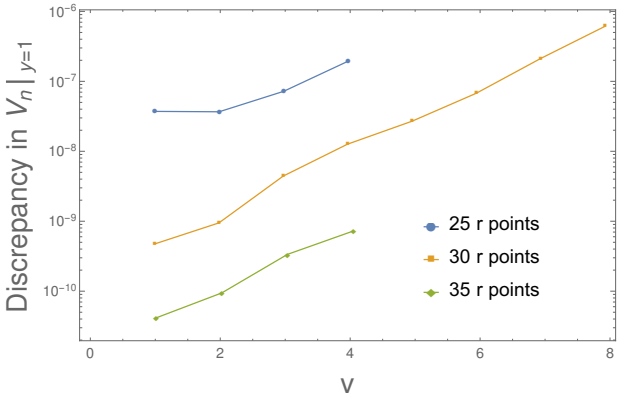

Fig. 6.7 A log plot of the maximum difference between the two methods of calculating $V_n|_{y=1}$ for the $a_0 = 0.7071$ solution. We vary the number of points in the r direction and use 40 points in the y direction. r and y are coordinates used in the numerics in place of x and ξ, and are defined in the Appendix.

from the boundary). The expansion should vanish, but this is not enforced explicitly by the numerical scheme. We have checked that although the expansion is non-zero, it indeed remains small in all of our results. We can be even more explicit about its effect on the numerical error in our solution by comparing the two different ways of solving for $d_t\chi$. Recall that we had two choices of boundary condition. We could evolve boundary data at $\xi = 1$ (the approach we actually took) or we could explicitly impose a vanishing expansion at $\xi = 0$ to get a boundary condition for $d_t\chi$ at $\xi = 0$. In our numerics, $d_t\chi$ is replaced by the function V_n (see Appendix), and comparing the two different ways of calculating V_n at the boundary can therefore give us an estimate of the size of the numerical error. In Fig. 6.7, we plot the maximum size of the difference between the two methods of calculating V_n against v for our $a_0 = 0.7071$ solution. As a test on convergence, we have repeated this for different grid sizes.

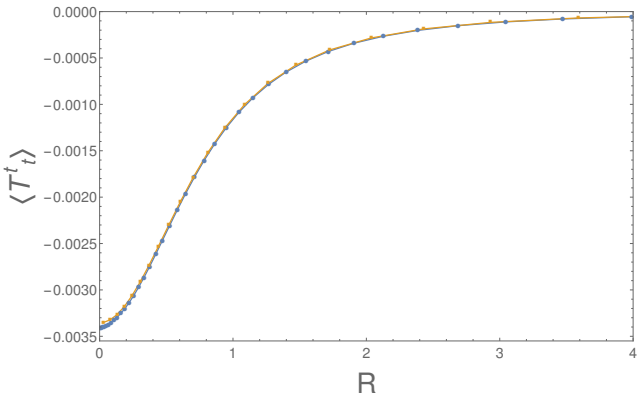

Fig. 6.8 Comparing the numerical results of [35] (blue disks) and the current simulations (orange squares) for $a_0 = 0.4243$.

As a further check on the accuracy of our numerical scheme, we can compare the end-point of our sub-critical solutions to the stationary solutions obtained in [35]. We make this comparison in Figure 6.8, plotting the tt component of the boundary stress tensor in the two cases, and finding good agreement. The small discrepancy can be explained by the fact that our solution has not yet completely settled down.

6.5 Discussion

We have presented numerical evidence that the WCCC is violated if we impose the boundary condition 6.3 with a sufficiently large a and $\gamma = 1$ (corresponding to a $1/R$ decay in the potential near infinity on the boundary). Based on the stationary solutions in [35], we should also expect to see similar behaviour for faster decays (with $\gamma \geq 1$). It would be interesting to check this in the time dependent solutions as well. However, when the decay is faster we have not been able to keep our super-critical numerical solutions stable for long enough to observe what will happen. Part of the problem is that $a_{\max}$ grows rapidly with γ so that solutions with $a > a_{\max}$ necessarily contain large gradients which are difficult for the numerical scheme to resolve. We must rely on the evidence from the stationary solutions to argue why the WCCC is likely to be violated with faster decays as well.

One might worry that since we are adding energy to the system, it will heat up, so that our zero temperature boundary conditions at $x = 0$ will no longer be consistent (see for instance [34]). However, raising the temperature of a planar horizon requires an infinite amount of energy and we have checked that the total energy we add to the system is finite. Checking this is not entirely straightforward. The boundary energy density $\langle T_{tt} \rangle$ at large R exhibits a $1/R$ decay, because of the contribution from outgoing spherical waves, and naively integrating

this over a constant v slice does give a divergent result. However, we find that this $1/R$ tail decays exponentially with v, so that integrating over a constant t slice gives a result which is both finite and bounded as $t \to \infty$. This implies that the total energy added to the system is actually finite, as required.

Another concern is whether or not there is a positivity of energy theorem for these space times. This was the most important problem with the numerical results of Chapter 5. This time though, even with the time dependent boundary conditions we impose, the metric and gauge field satisfy the required conditions for the proof of the positivity of energy theorem detailed in [25]. This result does not follow immediately from the coordinates used in the numerics. However, one can show that if we transform our boundary expansion to Fefferman-Graham coordinates [19], the approach to pure AdS in standard Poincaré coordinates is compatible with those required in [25].

One might also wonder whether our counter-examples to the WCCC are generic, since $\partial/\partial\phi$ is a Killing vector field everywhere in the bulk. Recall that it is straightforward to violate the WCCC if you are allowed to fine tune the initial conditions. However, weakening this symmetry assumption is unlikely to change our conclusions. This is because even if $\partial/\partial\phi$ is only an asymptotically Killing vector field, no static solutions with a simply connected horizon were found in [35] for $a > a_{\max}$.

Finally, it is interesting to ask what will happen to our examples if charged fields are included in our action. The fact that we had no charged matter was a crucial ingredient in our argument for why we expected to see cosmic censorship violation. This is because we needed to rule out the formation of hovering black holes. Stationary solutions containing hovering black holes exist for arbitrarily large amplitude, and so they could provide an alternative, non-singular, end point for our time dependent solutions when charged matter is present. It seems likely that some critical charge to mass ratio is necessary for these hovering black holes (which have an extremal horizon) to form, so that below this ratio the WCCC is still violated, while above this, it is saved. Of course at the classical level one can always set the charged matter fields to zero in the initial conditions and recover our solutions, but the initial data would in that case be fine tuned.

If this interpretation is correct, it is reminiscent of the Weak Gravity Conjecture (WGC) [55], one of the Swampland conjectures in String Theory. The WGC claims that any consistent quantum theory of gravity with a gauge interaction must contain particles which are charged under that interaction, and the charge to mass ratio must be above some critical threshold [1]. This raises the interesting question: could it be that the WCCC is only violated when the WGC conditions are violated as well? In other words, do our WCCC violations only work when our action cannot be realised as the low energy limit of a consistent theory

of quantum gravity? We also saw hints of this idea in Chapter 5. Even if positivity of energy holds and our vacuum examples violate the WCCC, it seems unlikely that they can be embedded in a consistent quantum theory of gravity, since the dual CFT has energy unbounded below. We discuss these ideas in detail in the next Chapter.

Chapter 7

A Connection between Weak Gravity and Cosmic Censorship?

In the previous Chapter, we suggested that it might only be possible to violate the WCCC in theories which cannot be realised as the low energy limit of a consistent theory of quantum gravity. In particular, if the WGC is true, then our electromagnetic examples cannot be completed into quantum gravity in the UV unless we also include charged matter with a sufficiently large charge (relative to its mass). However, it seems likely that if we were to do this, then the WCCC would no longer be violated in our examples. It is interesting to investigate this potential connection [55] between the two conjectures further. One way to test it would be to compare the lower bounds on the charge in the two conjectures to see if they really do match.

In the first part of this Chapter, we review the WGC. In the second part, we present numerical evidence that the two charge to mass ratios do indeed match, and we discuss the implications of this result.

7.1 The Weak Gravity Conjecture

The WGC is one of the so called "Swampland" conjectures of String Theory, reviewed in [47]. We now summarise the key points. The swampland conjectures seek to divide the space of apparently self-consistent low energy effective QFTs into those which *can* be completed into quantum gravity in the UV (the landscape) from those which cannot (the swampland). In particular, the WGC (first proposed in [1]) asserts that any theory with a $U(1)$ gauge interaction must contain particles which are charged under that interaction. Furthermore, the charge of at least one of these particles must be above some critical threshold, typically set

by the requirement that extremal charged black holes should be able to decay. This means that although there exist apparently self-consistent effective theories which violate these conditions (Einstein-Maxwell theory being one example), if they are going to be completed in the UV into a theory of quantum gravity, then charged particles must appear at some energy scale along the way. We should consider how this would affect our results from the previous chapter.

There are two kinds of arguments that one can use to arrive at the swampland conjectures. First, one can explicitly construct string theory vacua to obtain examples of effective theories which lie in the landscape, and then look for features which all such theories seem to have in common. If a single example was found which violated one of the swampland conjectures, then that would be enough to refute the conjecture, so every example which is consistent with the conjectures is at least weak evidence in their favour. However, an obvious drawback with this approach is that constructing these vacua is very difficult, and the ones which are known have very special properties. For example, they are usually supersymmetric. It could be that the swampland conjectures only apply to these special vacua, and are not true of the landscape generally. The second approach is to use quantum gravity arguments directly in the low energy theory, typically relating to black holes. We now briefly review one of the main arguments of this kind that has been put forward to support the WGC.

To motivate the WGC, it is common to begin with the claim that *there should be no exact global symmetries in quantum gravity* [63]. This claim can itself be viewed as a kind of swampland conjecture, in that it puts a constraint on which low energy theories are acceptable. It can be defended with arguments based on the behaviour of black holes. The basic idea is that any global symmetry should have an associated conserved charge, but that the Hawking evaporation process for black holes will not respect this conservation rule, since the charge of the black hole under this symmetry should not affect the geometry of its horizon. The same problem does not occur with gauge symmetries, since in that case the charge of the black hole can be measured outside of the horizon (from the flux of the gauge field) and will therefore influence the evaporation process so that charge conservation is respected.

If we accept this argument, then we have ruled out the existence of global symmetries in quantum gravity. The intuition behind the WGC is that gauge symmetries, although not forbidden, can still be constrained by applying similar black hole arguments. In particular, there will be constraints on the gauge coupling. The WGC says that charged particles should exist, and it places a lower bound on the charge that at least one of the charged fields must obey. This comes from the requirement that charged black holes should be able to decay. If charged black holes were unable to decay, then the theory would contain stable charged "remnants", and it has been suggested that this would be problematic. It is still unclear

whether remnants necessarily lead to an inconsistency in a theory of quantum gravity, but supposing that they do, it is then fairly straightforward to calculate the lower bound on the charge. This is because the charge of the black holes themselves is bounded above by the mass, through the extremality bound. In $3+1$ dimensions with no cosmological constant we have

$$Q \leq M \tag{7.1}$$

where Q and M are the charge and mass of the black hole respectively. When the black hole emits particles, through either thermal emission or Schwinger pair production, its new charge and mass must still obey the above inequality. This means that in the case where the black hole is initially extremal, saturating the inequality, the particles it emits must obey the opposite inequality

$$q \geq m. \tag{7.2}$$

This is the WGC bound on the charge in $3+1$ dimensions with no cosmological constant.

Since the counter-examples to the WCCC presented so far have all been asymptotically AdS, we are interested in the WGC bound with negative cosmological constant. Again, we can derive this bound from the requirement that charged extremal black holes should be able to decay. Unlike in asymptotically flat space where black holes are only unstable once quantum effects are taken into account, in asymptotically AdS space the instability can be seen at the classical level. This is because of the reflecting boundary conditions, which lead to the superradiant instability. We can therefore obtain the AdS WGC bound based on the requirement that extremal charged black holes should be unstable to the classical superradiant instability.

To stay as close as possible to the original weak gravity conjecture, we will consider an arbitrarily small black hole[1]. The charged matter we consider is a massive scalar field of charge q and mass m. The general spherically symmetric charged black hole in AdS is the AdS Reissner-Nordstrom black hole:

$$ds^2 = -f(r)dt^2 + \frac{dr^2}{f(r)} + r^2 d\Omega^2, \qquad A = \mu\left(1 - \frac{r_+}{r}\right)dt \tag{7.3}$$

where

$$f(r) = \frac{r^2}{L^2} + 1 + \frac{\mu^2 r_+^2}{r^2} - \frac{r_+}{r}\left(\frac{r_+^2}{L^2} + 1 + \mu^2\right). \tag{7.4}$$

[1]Note that even an uncharged black hole is quantum mechanically stable in AdS when sufficiently large, but this is not supposed to present a problem for the WGC.

The event horizon lies at $r = r_+$ (the largest real root of $f(r)$) and the Hawking temperature is given by

$$T_H = \frac{L^2 - L^2\mu^2 + 3r_+^2}{4L^2\pi r_+}. \tag{7.5}$$

We are interested in extremal black holes which have $\mu = \sqrt{1 + r_+^2/L^2}$ so that $T_H = 0$. Superradiant scattering occurs for modes with [53, 23]

$$0 < \omega < q\mu \tag{7.6}$$

so we need to know which values of ω are allowed for a small black hole. In other words, we need to know what the quasinormal mode spectrum looks like. If the black holes are small, two decoupled sectors of quasinormal mode excitations exist: one whose imaginary part grows infinitely negative as the size of the hole decreases, and another whose imaginary part drops to zero as the black hole becomes smaller and whose real part approaches the normal modes of AdS [4, 54]. It is the latter type that is of interest to us. In the approximation where the extremal black hole is very small, the quasinormal mode with the smallest real part will have

$$\omega L = \Delta + o(r_+/L) \tag{7.7}$$

where

$$\Delta = \frac{3}{2} + \sqrt{\frac{9}{4} + L^2m^2}. \tag{7.8}$$

If we substitute this into the inequality 7.6, and take the $r_+ \to 0$ limit we find the AdS WGC bound

$$q \geq \frac{\Delta}{L}. \tag{7.9}$$

Note that this reduces to the flat space bound in the $L \to \infty$ limit.

7.2 Testing the WGC-WCCC Connection

To test the connection between the WGC and WCCC, we should add a charged field to our electromagnetic examples to see if this can prevent the formation of a naked singularity. In particular, if there turns out to be a minimum charge necessary to avoid a naked singularity, we want to compare this to the bound given to us by the WGC: $q \geq q_W = \frac{\Delta}{L}$. Including a charged massive scalar field in our action gives us

$$S = \frac{1}{16\pi}\int d^4x\sqrt{-g}\left(R + \frac{6}{L^2} - F^{ab}F_{ab} - 4(D_a\Phi)(D^a\Phi)^\dagger - 4m^2\Phi\Phi^\dagger\right) \tag{7.10}$$

where $D_a = \nabla_a - iqA_a$ is the gauge covariant derivative. This gives rise to the equations of motion:

$$R_{ab} + \frac{3}{L^2} g_{ab} = 2\left(F_a^c F_{bc} - \frac{g_{ab}}{4} F_{cd}F^{cd}\right) + 2(D_a\Phi)(D_b\Phi)^\dagger + 2(D_a\Phi)^\dagger(D_b\Phi) + 2m^2 g_{ab}\Phi\Phi^\dagger \tag{7.11}$$

$$\nabla_a F_b^a = iq\left((D_b\Phi)\Phi^\dagger - (D_b\Phi)^\dagger\Phi\right) \tag{7.12}$$

$$D_a D^a\Phi = m^2\Phi. \tag{7.13}$$

Ideally, we would repeat the time dependent calculations from Chapter 6 with these equations of motion. We might then expect to see the formation of hovering black holes. However, the time dependent numerics are challenging, and it turns out that we can make some progress just by looking at stationary solutions. The idea is that once we have a scalar field, not only might we be able to form hovering black holes, but also the stationary solutions with connected horizon might now be unstable to forming scalar hair. If (1) they are unstable, and (2) these hairy solutions persist for arbitrarily large amplitude, then this would suggest that naked singularities are avoided, whether or not hovering black holes form. Fortunately, we are able to check (1) and (2) just by examining stationary solutions. In the next section we present our numerical results and show that remarkably, (1) and (2) are both true for a sufficiently large value of the charge. The required charge agrees precisely with the WGC bound.

7.2.1 Results

Stationary solutions to the equations of motion arising from 7.10 were obtained using the DeTurck method, for boundary electric field profiles of the form

$$A_\partial = \frac{adt}{(1 + r^2/l^2)^{n/2}}. \tag{7.14}$$

Again, only the product al is physically meaningful, so we set $l = 1$ without loss of generality. First, we recover the stationary solutions already obtained in [35] with connected horizon and no scalar field. We now want to test if these solutions are unstable to forming scalar hair through the mechanism proposed in [28, 30]. In order to do this, we make use of the fact that a static normalizable mode usually marks the transition between stable and unstable solutions. We will search for such zero modes following the same strategy as in [36, 12]. We take our stationary solutions as a fixed background, and look for time independent solutions of Equation 7.13 on this background. In the stationary solutions, time derivatives all vanish

and the only non-zero component of the gauge field is A_t. Equation 7.13 therefore reduces to

$$\left(\nabla_a \nabla^a - m^2\right) \Phi = q^2 A_a A^a \Phi. \tag{7.15}$$

This can be viewed as a generalized eigenvalue problem, with eigenfunction Φ and eigenvalue q^2. For a given electric field profile, and given value of the scalar field mass m, we can determine the smallest eigenvalue $q_{\min}$. We will then want to interpret this as the smallest charge required for the stationary solution to be unstable to forming scalar hair.

We also need to specify the boundary conditions on the scalar field. The leading order behaviour of the scalar field near the boundary is given, in Fefferman-Graham coordinates, by

$$\Phi = \Phi_- z^{\delta_-} + \Phi_+ z^{\delta_+} + ... \tag{7.16}$$

where

$$\delta_\pm = \frac{3}{2} \pm \sqrt{\frac{9}{4} + L^2 m^2}. \tag{7.17}$$

Note that Δ, as defined in Equation 7.8, is equal to δ_+. Typically, we set Φ_- to zero as our scalar field boundary condition. The only exception is when we want to work with $\Delta < \frac{3}{2}$. We can make sense of this by identifying Δ with δ_- instead of δ_+, and then setting Φ_+ to zero as a boundary condition. This works provided that $\Delta \geq \frac{1}{2}$.

With this set-up, we have computed $q_{\min}$ for various profiles, labelled by n, and amplitudes, a, with both $\Delta = 2$ and $\Delta = 4$. The results are displayed in Figures 7.1 and 7.2. To facilitate comparison with the WGC bound, we plot $q_{\min}/q_W$ on the vertical axis and place a dotted horizontal line at $q_{\min}/q_W = 1$. Each curve on the plot terminates at $a_{\max}$, where stationary solutions with connected horizon and no scalar field no longer exist. In every case, we see that the curve dips below the dotted line before reaching $a_{\max}$. This means that if the WGC bound is obeyed, so $q > q_W$, and we slowly increase the amplitude, the Einstein-Maxwell stationary solution appears to become unstable to forming scalar hair before it becomes singular. The resulting hairy solutions might themselves give rise to singular behaviour, but these results suggest that the WGC bound is at least sufficient to avoid the kind of naked singularity we saw in the previous Chapter.

We should now check that these zero modes really do mark the boundary between stable and unstable solutions. To do this we include harmonic time dependence $e^{-i\omega t}$ in the scalar perturbation and compute the lowest quasinormal mode frequency for each a. We take $\Delta = 4$, and set $q = q_W$ since larger q are more likely to induce instabilities. Since the zero mode has $\omega = 0$, as we change a at fixed charge, both the real and imaginary parts of the lowest quasinormal mode frequency must pass through zero. If $\mathrm{Im}\omega$ becomes positive, the mode

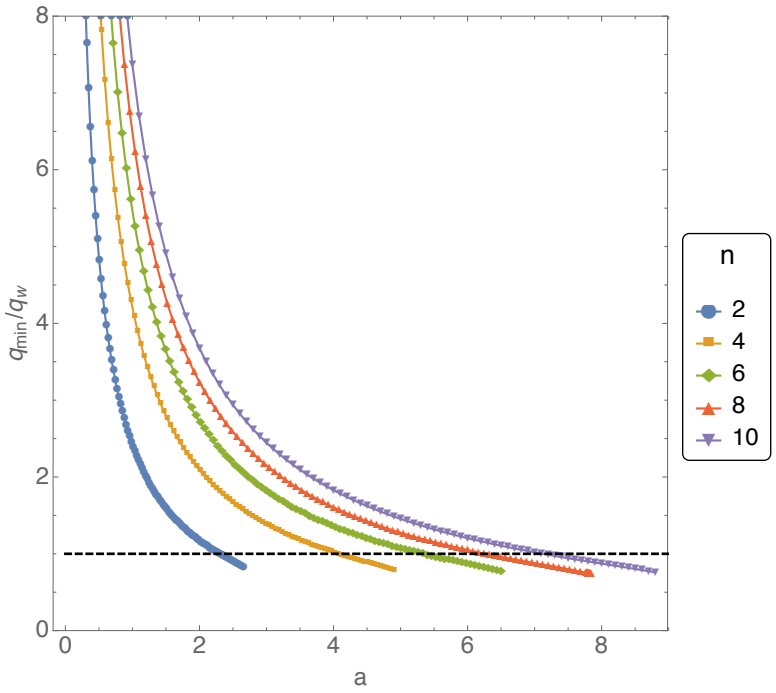

Fig. 7.1 The minimum charge, q_{min}, needed for a zero-mode as a function of the amplitude a, plotted for several different profiles. From bottom to top we have $n = 2,4,6,8,10$, respectively. The horizontal dashed line represents the weak gravity bound $q_{\text{min}}/q_W = 1$. These curves were determined for $\Delta = 2$.

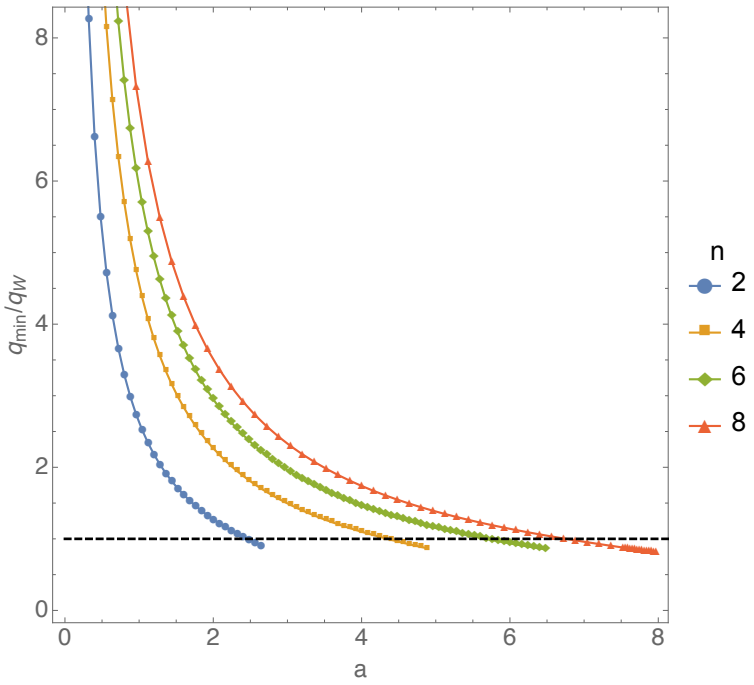

Fig. 7.2 The minimum charge, $q_{\min}$, needed for a zero-mode as a function of the amplitude a, plotted for several different profiles. From bottom to top we have $n = 2,4,6,8,10$, respectively. The horizontal dashed line represents the weak gravity bound $q_{\min}/q_W = 1$. These curves were determined for $\Delta = 4$.

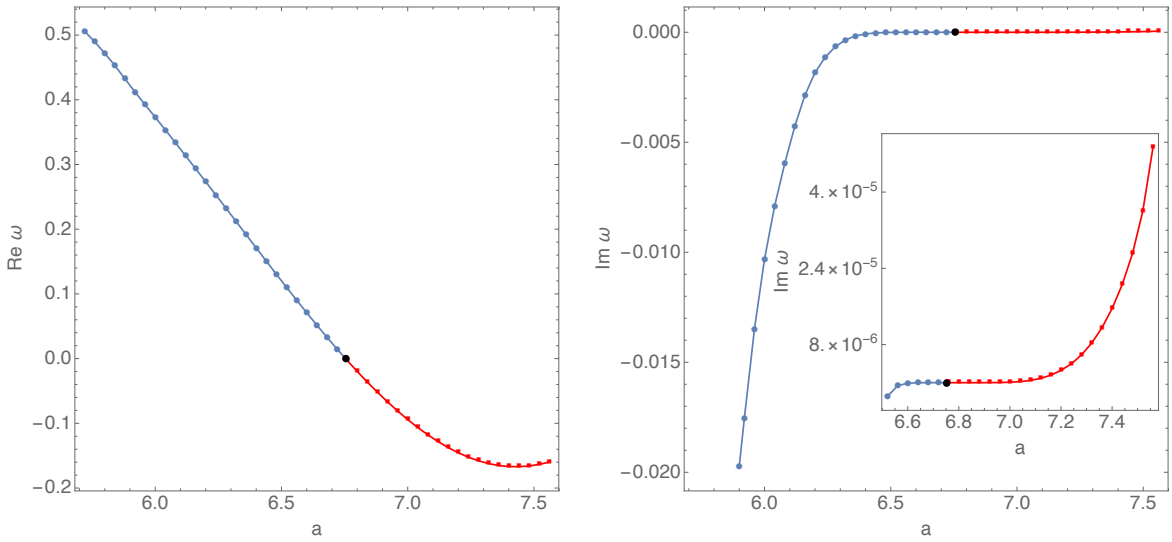

Fig. 7.3 The lowest quasinormal mode frequency for $n = 8, \Delta = 4, q = q_W$. The black dot denotes the zero mode. The red dots have the opposite sign of ω from the blue dots. The insert on the right plots the data on a logarithmic scale, clearly showing that Imω becomes positive after the zero mode, so the solution without the scalar field becomes unstable.

becomes unstable. As Figure 7.3 shows, this is exactly what we find. The location of the zero mode is shown as a black dot, and Imω changes sign there. Since Imω is small near the zero mode, the instability sets in slowly. We believe that the instability will set in faster for larger values of q.

We should also check whether the same story will hold for all values of the scalar field mass. We have repeated the calculation of the zero-mode charge $q_{\rm min}$ for many values of Δ. Since the lowest value of $q_{\rm min}$ always occurs for $a = a_{\rm max}$, we keep $a = a_{\rm max}$ and compute $q_{\rm min}$ for various Δ for the $n = 8$ profile. The results are plotted in Figure 7.4. The fact that $q_{\rm min}/q_W$ is always less than one means that the situation is always qualitatively the same as the previous cases.

We have now seen evidence that if the WGC bound is obeyed, the Einstein-Maxwell stationary solutions with connected horizon become unstable to forming scalar hair. The next question is: how do these hairy solutions behave? In particular, do non-singular hairy solutions persist for arbitrarily large amplitude, thereby avoiding naked singularity formation? Or might they too become singular? We have constructed the hairy stationary solutions numerically for $n = 8, \Delta = 2$ with various different charges and amplitudes (other values of n and Δ have also been tried and give similar results). We find that for certain values of the charge, there is still a maximum amplitude in the hairy solutions, with the Kretschmann diverging as this maximum is approached. It seems that the formation of scalar hair is not necessarily enough to avoid naked singularity formation. However, we find that as

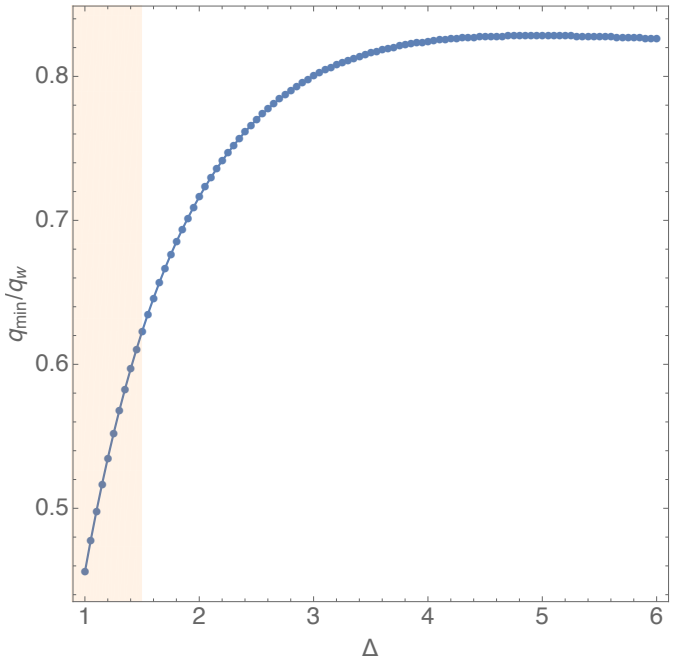

Fig. 7.4 $q_{\min}/q_W$ as a function of $\Delta \geq 1$ plotted for $n = 8$ and $a = a_{\max}$. The orange region indicates the region of moduli space where we used alternative boundary conditions.

the charge increases, the maximum amplitude increases as well. Remarkably, when the charge exceeds q_W, there is no longer a maximum amplitude at all, and so there seems to be no naked singularity. We present these results in Figure 7.5. The blue curve depicts the stationary solutions we found before, ending at $a_{\max}$. The orange curve shows the threshold for existence of the hairy solutions. For each value of the amplitude, we decrease the charge until the solution becomes singular (the Kretschmann diverges), and the place where that happens becomes a point on the orange curve. Hairy solutions therefore only exist above this curve. The orange curve appears to approach the dotted line $q_{\min}/q_W = 1$ as $a \to \infty$, so there is no maximum amplitude if and only if the WGC bound is respected. The WGC condition appears to be both necessary and sufficient for the WCCC to hold.

There is one caveat that must be added to this result. We have only looked at stationary solutions, and we have not said anything about hovering black holes. This means that although we can be confident that the WGC bound is sufficient to avoid a violation of the WCCC, it may not be necessary. We cannot rule out the possibility that hovering black holes might form even when $q < q_W$. This could also prevent the formation of a naked singularity. We would need to compute the full time dependent solution to determine whether or not this happens.

Another problem with the above results is that we always work with $n \geq 2$. This is because the numerics for the stationary solutions are easier to handle. However, the time dependent

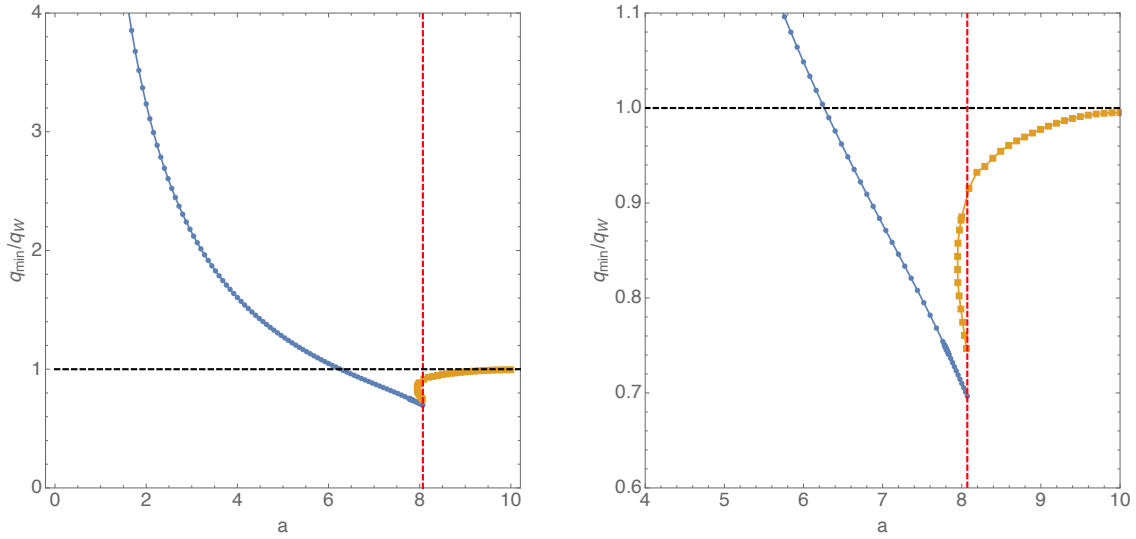

Fig. 7.5 Phase diagram of solutions for $n = 8$ and $\Delta = 2$. The dashed vertical line denotes $a = a_{\max}$. Solutions with $\Phi \neq 0$ exist above the (blue and yellow) line connecting the dots, and $\Phi \to 0$ along this line for $a < a_{\max}$, but develops singularities along the line for $a > a_{\max}$. The right panel shows a blowup of part of the left panel.

results of the previous chapter, which confirmed the formation of a naked singularity without charged matter, had $n = 1$. This is because that turned out to be the numerically simpler choice in that context. We expect the $n > 1$ profiles to behave similarly in the time dependent case, based on the corresponding stationary solutions. Nevertheless, it is unfortunate that we cannot compare the results of this Chapter directly to the results of the previous one, using the same value of n.

7.3 Conclusion

We have seen evidence for a close connection between the WGC and the WCCC. If the WGC is true, then an effective theory can only be completed into a consistent quantum gravity theory in the UV if it contains a charged particle with $q > q_W$. Remarkably, the WCCC in $3+1$ dimensional asymptotically AdS space appears to only hold if that same condition is true. This connection has been further supported by the work of [37], which found evidence for this connection in a wider class of theories, first including a dilaton and then including multiple gauge fields. It is tempting to conclude that violations of the WCCC are possible, but *only in theories which do not admit a UV completion in quantum gravity*.

The vacuum examples of Chapter 5 are consistent with this conclusion. Recall that they could be interpreted in one of two ways. If no positivity of energy theorem applies to these

examples, then the rotational analogue of our electromagnetic boundary condition *fails* to violate the WCCC. This then poses no problems for our conclusion. If on the other hand a positivity of energy theorem does apply, the vacuum examples *may* violate the WCCC, but only when the boundary metric contains an ergoregion. In this case the dual CFT would have a spectrum of energy states unbounded below. This would then be a new, independent, example where the WCCC can be violated only when there is no good quantum gravity description in the UV. This would be even stronger evidence in support of our conclusion.

What about the violations of the WCCC which do not fit into this picture? In Chapter 2 we saw two examples where the WCCC is probably violated but a consistent quantum gravity description presumably does exist: the Gregory-Laflamme instability in higher dimensions, and the superradiant instability in asymptotically AdS spaces (including in $3+1$ dimensions). However, the naked singularities arising in these examples are "small". The curvature grows arbitrarily large, but only in an arbitrarily small region of the space time. It is worth pointing out that we also expect to see these kind of naked singularities in $3+1$ dimensional asymptotically flat space as well. They are not present in the classical theory, and do not arise during gravitational collapse (so are unlikely to have astrophysical relevance), but once quantum effects are taken into account we do expect black holes to become unstable and eventually evaporate. At the end of this process, we would expect quantum gravity effects to become visible to distant observers. However, the curvatures would again only be large in a small region of the space time. This is in contrast to our examples, where the curvature grows large over a large region of the space time.

With this in mind, we can propose a new, weakened, statement of the WCCC.

Conjecture 7.3.1. *The maximal evolution of complete initial data should contain no "large" naked singularities if the theory admits a consistent UV completion in quantum gravity.*

This conjecture has been further explored in [18], where holographic arguments were used to derive the Penrose inequality in AdS. This is an explicit example of how quantum gravity considerations can enforce the WCCC in classical GR. Their derivation also works in higher dimensions, where the WCCC in the traditional sense fails, but the weakened form may still hold. If this conjecture *is* true, it is interesting to ask why. It seems to be pointing to something deep about the nature of quantum gravity.

References

[1] Arkani-Hamed, N., Motl, L., Nicolis, A., and Vafa, C. (2007). The String landscape, black holes and gravity as the weakest force. *JHEP*, 06:060.

[2] Ashtekar, A. and Magnon-Ashtekar, A. (1975). Sublimation d'ergospheres. *C. R. Acad. Sci. Paris*, 281A(875).

[3] Balasubramanian, K. and Herzog, C. P. (2014). Losing Forward Momentum Holographically. *Class. Quant. Grav.*, 31:125010.

[4] Berti, E. and Kokkotas, K. D. (2003). Quasinormal modes of Reissner-Nordstrom-anti-de Sitter black holes: Scalar, electromagnetic and gravitational perturbations. *Phys. Rev.*, D67:064020.

[5] Bondi, H., van der Burg, M. G. J., and Metzner, A. W. K. (1962). Gravitational waves in general relativity. 7. Waves from axisymmetric isolated systems. *Proc. Roy. Soc. Lond.*, A269:21–52.

[6] Cardoso, V., Dias, Ó. J. C., Hartnett, G. S., Lehner, L., and Santos, J. E. (2014). Holographic thermalization, quasinormal modes and superradiance in Kerr-AdS. *JHEP*, 04:183.

[7] Chesler, P. M. and Lowe, D. A. (2019). Nonlinear evolution of the AdS_4 black hole bomb. *Phys. Rev. Lett.*, 122(18):181101.

[8] Choptuik, M. W. (1993). Universality and scaling in gravitational collapse of a massless scalar field. *Phys. Rev. Lett.*, 70:9–12.

[9] Christodoulou, D. (1984). Violation of cosmic censorship in the gravitational collapse of a dust cloud. *Communications in Mathematical Physics*, 93(2):171–195.

[10] Christodoulou, D. (1994). Examples of Naked Singularity Formation in the Gravitational Collapse of a Scalar Field. *Annals of Mathematics*, 140(3):607–653.

[11] Christodoulou, D. (1998). The instability of naked singularities in the gravitational collapse of a scalar field. *arXiv Mathematics e-prints*, page math/9901147.

[12] Costa, M. S., Greenspan, L., Penedones, J., and Santos, J. E. (2017). Polarised Black Holes in ABJM. *JHEP*, 06:024.

[13] Crisford, T., Horowitz, G. T., and Santos, J. E. (2018). Testing the Weak Gravity - Cosmic Censorship Connection. *Phys. Rev.*, D97(6):066005.

[14] Crisford, T., Horowitz, G. T., and Santos, J. E. (2019). Attempts at vacuum counterexamples to cosmic censorship in AdS. *JHEP*, 02:092.

[15] Crisford, T. and Santos, J. E. (2017). Violating the Weak Cosmic Censorship Conjecture in Four-Dimensional Anti–de Sitter Space. *Phys. Rev. Lett.*, 118(18):181101.

[16] Dafermos, M., Holzegel, G., and Rodnianski, I. (2016). The linear stability of the Schwarzschild solution to gravitational perturbations.

[17] Emparan, R. and Reall, H. S. (2002). A Rotating black ring solution in five-dimensions. *Phys. Rev. Lett.*, 88:101101.

[18] Engelhardt, N. and Horowitz, G. T. (2019). A Holographic Argument for the Penrose Inequality in AdS.

[19] Fefferman, C. and Graham, C. R. (2007). The ambient metric. *arXiv e-prints*, page arXiv:0710.0919.

[20] Figueras, P., Kunesch, M., and Tunyasuvunakool, S. (2016). End Point of Black Ring Instabilities and the Weak Cosmic Censorship Conjecture. *Phys. Rev. Lett.*, 116(7):071102.

[21] Friedman, J. L. (1978). Ergosphere instability. *Communications in Mathematical Physics*, 63(3):243–255.

[22] Geroch, R. P. and Horowitz, G. T. (1979). Global structure of spacetimes. In *General Relativity: An Einstein Centenary Survey*, pages 212–293.

[23] Gibbons, G. W. (1975). Vacuum polarization and the spontaneous loss of charge by black holes. *Comm. Math. Phys.*, 44(3):245–264.

[24] Gibbons, G. W. (1997). Collapsing shells and the isoperimetric inequality for black holes. *Class. Quant. Grav.*, 14:2905–2915.

[25] Gibbons, G. W., Hull, C. M., and Warner, N. P. (1983). The Stability of Gauged Supergravity. *Nucl. Phys.*, B218:173.

[26] Green, S. R., Hollands, S., Ishibashi, A., and Wald, R. M. (2016). Superradiant instabilities of asymptotically anti-de Sitter black holes. *Class. Quant. Grav.*, 33(12):125022.

[27] Gregory, R. and Laflamme, R. (1993). Black strings and p-branes are unstable. *Phys. Rev. Lett.*, 70:2837–2840.

[28] Gubser, S. S. (2008). Breaking an Abelian gauge symmetry near a black hole horizon. *Phys. Rev.*, D78:065034.

[29] Gubser, S. S., Klebanov, I. R., and Polyakov, A. M. (1998). Gauge theory correlators from noncritical string theory. *Phys. Lett.*, B428:105–114.

[30] Hartnoll, S. A., Herzog, C. P., and Horowitz, G. T. (2008). Building a Holographic Superconductor. *Phys. Rev. Lett.*, 101:031601.

[31] Hawking, S. W. and Page, D. N. (1983). Thermodynamics of black holes in anti-de Sitter space. *Communications in Mathematical Physics*, 87(4):577–588.

[32] Hawking, S. W. and Reall, H. S. (2000). Charged and rotating AdS black holes and their CFT duals. *Phys. Rev.*, D61:024014.

[33] Headrick, M., Kitchen, S., and Wiseman, T. (2010). A New approach to static numerical relativity, and its application to Kaluza-Klein black holes. *Class. Quant. Grav.*, 27:035002.

[34] Horowitz, G. T., Iqbal, N., and Santos, J. E. (2013). Simple holographic model of nonlinear conductivity. *Phys. Rev.*, D88(12):126002.

[35] Horowitz, G. T., Iqbal, N., Santos, J. E., and Way, B. (2015). Hovering Black Holes from Charged Defects. *Class. Quant. Grav.*, 32:105001.

[36] Horowitz, G. T. and Santos, J. E. (2013). General Relativity and the Cuprates. *JHEP*, 06:087.

[37] Horowitz, G. T. and Santos, J. E. (2019). Further evidence for the weak gravity - cosmic censorship connection.

[38] Horowitz, G. T., Santos, J. E., and Way, B. (2016). Evidence for an Electrifying Violation of Cosmic Censorship. *Class. Quant. Grav.*, 33(19):195007.

[39] Isenberg, J., Maxwell, D., and Pollack, D. (2005). A Gluing construction for non-vacuum solutions of the Einstein constraint equations. *Adv. Theor. Math. Phys.*, 9(1):129–172.

[40] Kang, G. (1997). Quantum aspects of ergoregion instability. *Phys. Rev.*, D55:7563–7573.

[41] Kerr, R. P. (1963). Gravitational Field of a Spinning Mass as an Example of Algebraically Special Metrics. *Phys. Rev. Lett.*, 11:237–238.

[42] Lehner, L. and Pretorius, F. (2010). Black Strings, Low Viscosity Fluids, and Violation of Cosmic Censorship. *Phys. Rev. Lett.*, 105:101102.

[43] Maldacena, J. (2012). The Gauge/gravity duality. In Horowitz, G. T., editor, *Black holes in higher dimensions*, pages 325–347.

[44] Maldacena, J. M. (1999). The Large N limit of superconformal field theories and supergravity. *Int. J. Theor. Phys.*, 38:1113–1133. [Adv. Theor. Math. Phys.2,231(1998)].

[45] Matzner, R. A., Seidel, H. E., Shapiro, S. L., Smarr, L., Suen, W.-M., Teukolsky, S. A., and Winicour, J. (1995). Geometry of a Black Hole Collision. *Science*, 270(5238):941–947.

[46] Niehoff, B. E., Santos, J. E., and Way, B. (2016). Towards a violation of cosmic censorship. *Class. Quant. Grav.*, 33(18):185012.

[47] Palti, E. (2019). The Swampland: Introduction and Review.

[48] Penrose, R. (1965). Gravitational collapse and space-time singularities. *Phys. Rev. Lett.*, 14:57–59.

[49] Penrose, R. (1969). Gravitational collapse: The role of general relativity. *Riv. Nuovo Cim.*, 1:252–276. [Gen. Rel. Grav.34,1141(2002)].

[50] PENROSE R. and FLOYD R. M. (1971). Extraction of Rotational Energy from a Black Hole. *Nature Physical Science*, 229:177.

[51] Schwarzschild, K. (1916). On the gravitational field of a mass point according to Einstein's theory. *Sitzungsber. Preuss. Akad. Wiss. Berlin (Math. Phys.)*, 1916:189–196.

[52] Sorce, J. and Wald, R. M. (2017). Gedanken experiments to destroy a black hole. II. Kerr-Newman black holes cannot be overcharged or overspun. *Phys. Rev.*, D96(10):104014.

[53] Starobinskii, A. A. (1973). Amplification of waves during reflection from a rotating "black hole". *JETP*, 37(1):28.

[54] Uchikata, N. and Yoshida, S. (2011). Quasinormal modes of a massless charged scalar field on a small Reissner-Nordstrom-anti-de Sitter black hole. *Phys. Rev.*, D83:064020.

[55] Vafa, C. (2016). We thank C. Vafa for pointing out this connection.

[56] Vishveshwara, C. V. (1970). Stability of the Schwarzschild Metric. *Phys. Rev. D*, 1:2870–2879.

[57] Wald, R. (1974). Gedanken experiments to destroy a black hole. *Annals of Physics*, 82(2):548–556.

[58] Wald, R. M. (1984). *General Relativity*. The University of Chicago Press.

[59] Wald, R. M. (1997). Gravitational collapse and cosmic censorship. In *Black Holes, Gravitational Radiation and the Universe: Essays in Honor of C.V. Vishveshwara*, pages 69–85.

[60] Whiting, B. F. (1989). Mode stability of the Kerr black hole. *Journal of Mathematical Physics*, 30(6):1301–1305.

[61] Winicour, J. (2009). Characteristic Evolution and Matching. *Living Rev. Rel.*, 12:3.

[62] Witten, E. (1998). Anti-de Sitter space and holography. *Adv. Theor. Math. Phys.*, 2:253–291.

[63] Witten, E. (2018). Symmetry and Emergence. *Nature Phys.*, 14:116–119.

[64] Zel'dovich, Y. B. (1972). Amplification of Cylindrical Electromagnetic Waves Reflected from a Rotating Body. *JETP*, 35(6):1085.

Appendix A

Further Details of the Zero Temperature Numerical Scheme

The numerical scheme used to produce the results in Chapter 6 closely followed the description given in Chapter 4, but with a few slight differences. We present these differences here, as well as providing some further details on exactly how the scheme was implemented. Throughout this Appendix we choose $L = c = 1$.

First, we use a different definition of the function χ_3 :

$$\chi(v,\rho,x) = -\log\rho + \left(\frac{x-\rho}{x}\right)^3 \chi_3(v,x). \tag{A.1}$$

The second difference is that instead of defining coordinates Z and X using Equations 4.24 and 4.25, we work with the coordinates y and r defined in terms of ρ and x as follows:

$$\rho^{-1} = \frac{1}{x}\left(1 + \frac{1-y^2}{2y^2}\right) \tag{A.2}$$

$$x = \frac{1-r^2}{\sqrt{r^2+(1-r^2)^2}}. \tag{A.3}$$

The AdS boundary then lies at $y = 1$, the horizon lies at $y = 0$, and the symmetry axis lies at $r = 0$. This coordinate definition means we expect all of our functions to contain only even powers of y, and so we used a doubled Chebyshev grid in the bulk radial direction as well (in Chapter 4 we explained how to use such a grid in the boundary direction).

With these differences, the functions that we actually numerically integrate can now be defined. We define these new functions below in terms of the original metric functions given in Chapter 4 (the new functions are given a subscript n). The main guiding principle is to

subtract off as much of the known asymptotic behaviour at the boundary as we can:

$$\beta(v,\rho,x) = -\chi_3(v,x) f(\rho^{-1},x)^3 + f(\rho^{-1},x)^3 \beta_n(v,y,r) \tag{A.4a}$$

$$U(v,\rho,x) = f(\rho^{-1},x)^2 (1-x^2) U_n(v,y,r) \tag{A.4b}$$

$$\frac{\partial A_v}{\partial \rho^{-1}}(v,\rho,x) = \left(\frac{f(\rho^{-1},x)}{x\rho^{-1}-1}\right)^2 x (E_z)_n(v,y,r) \tag{A.4c}$$

$$\begin{aligned} &V(v,\rho,x) - 1 \\ &= \left(\frac{x^3\rho^{-3} + 3(1-x\rho^{-1})^3 \chi_3(v,x)}{2\rho^{-1}(1-x\rho^{-1})^4}\right)^{-1} \left(\frac{e^{\frac{2(1-3x\rho^{-1}+3x^2\rho^{-2})\chi_3(v,x)}{x^3\rho^{-3}}} x\rho^{-1}}{1-x\rho^{-1}} dt\, \chi_n(v,y,r) \right. \\ &\qquad \left. - \partial_v \chi_3(v,x) \right) \end{aligned} \tag{A.4d}$$

$$\alpha(v,\rho,x) = -\log(1-x^2) + f(\rho^{-1},x)^2 \frac{2-x^2-x\sqrt{4-3x^2}}{2-2x^2} \alpha_n(v,y,r) \tag{A.4e}$$

$$\frac{\partial A_x}{\partial \rho^{-1}}(v,\rho,x) = \left(\frac{f(\rho^{-1},x)}{x\rho^{-1}-1}\right)^2 B_n(v,y,r) \tag{A.4f}$$

$$\frac{\partial A_x}{\partial v}(v,\rho,x) - \frac{\partial A_v}{\partial x}(v,\rho,x) = x^{-1}(E_r)_n(v,y,r) + \frac{1}{2}\frac{\partial A_x}{\partial \rho^{-1}}(V-1) \tag{A.4g}$$

$$\frac{\partial \alpha}{\partial v}(v,\rho,x) = f(\rho^{-1},x)^2 \frac{2-x^2-x\sqrt{4-3x^2}}{2-2x^2} dt\, \alpha_n(v,y,r) + \frac{1}{2}\frac{\partial \alpha}{\partial \rho^{-1}}(V-1) \tag{A.4h}$$

where

$$f(a,b) = \frac{(ab-1)(1+4(ab-1))}{(1+2(ab-1))^2}. \tag{A.5}$$